Volume 1 • Number 3 • March 2007
ISSN: 1557-7244

Journal of APPLIED PACKAGING RESEARCH

Aim and Scope

The *Journal of Applied Packaging Research* is an international forum for the dissemination of research papers, review articles, tutorials and news about innovative or emerging technologies for the packaging industry. The journal is targeted towards the broad packaging community including packaging scientists and engineers in industry or academic research and development, food scientists and technologists, materials scientists, mechanical engineers, industrial and systems engineers, toxicologists, analytical chemists, environmental scientists, regulatory officers, and other professionals who are concerned with advances in the development and applications of packaging.

JOURNAL OF APPLIED PACKAGING RESEARCH—Published quarterly—September, December, March and June by DEStech Publications, Inc., 1148 Elizabeth Ave. #2, Lancaster, PA 17601.

Indexed by Chemical Abstracts Service.

Subscriptions: Annual $299 (Print), $299 (Electronic) and $324 (Print and Electronic). Single copy price $89.50. Foreign subscriptions add $45 per year for postage.

(ISSN 1557-7244)

DEStech Publications, Inc.
1148 Elizabeth Avenue #2, Lancaster, Pennsylvania 17601, U.S.A.

CONTENTS

Research

RESEARCH

Effects of Secondary Packaging, Food Product Viscosity and Headspace on Impact Breakage of Glass Containers

NECLA DEMIR[1,*] and PETER J. VERGANO[2]
[1]*Süleyman Demirel University, Department of Food Engineering, Çünür, Isparta, Turkey, 32260*
[2]*Professor Emeritus, Clemson University, Packaging Science, Clemson, SC, USA*

ABSTRACT: Breakage, mostly due to impact, is the most serious disadvantage of glass containers used for foods. Drop tests were used to determine the effects of a corrugated cushion, headspace, and product viscosity on the susceptibility to impact breakage of glass containers filled with simulated foods as purposes of this study. Containers were abraded prior to filling and testing to diminish the effect of glass container strength variability. There was a significant decrease in breakage using a single piece of corrugated paperboard under the jars ($p < 0.01$). Mean breakage drop height increased from 23.06 to 33.43 cm with a cushion. Breakage increased significantly ($p < 0.1$) as headspace was increased from 0% to 5% or 10%. Jars with high viscosity contents (500 poise) had lower breakage than low (0.009 poise) or medium (4 poise) viscosity content jars ($p < 0.01$). No significant breakage difference was observed between low and medium viscosity content jars. An unusual breakage pattern, interpreted as a combination of point source and hydrodynamic breakage, was observed. The weakening effects of additional headspace and lower viscosity may be related to their contributing to cavitation forces produced upon impact.

INTRODUCTION

GLASS is one of the oldest and most widely used packaging materials. It has been produced since 7000 B.C. and currently accounts for a $20 billion a year industry in the USA alone. Glass has been limited in its applications by its tendency to brittle fracture although it has a remarkable history of meeting a range of consumer needs [1]. Glass containers are utilized to package and store a wide variety of foods, bever-

*Author to whom correspondence should be addressed. Email: ndemir@ziraat.sdu.edu.tr

1557-7244/07/03 131-18

ages, chemicals, pharmaceuticals, and cosmetics [2]. Soda-lime-silica glass is used almost exclusively for food containers where exceptional chemical durability and heat resistance are not required [3]. Compositions of soda lime glass for containers are SiO_2 70–74%; Na_2O-K_2O 13–16%; CaO–MgO 10–13%; BaO 0–7.5%; Al_2O 1.5–2.5% [4]. Due to its amorphous structure, glass is brittle, and glass breaks due to an applied tensile stress [5]. A smooth surface on a bottle will withstand stresses of 100,000 psi or more. When the surface becomes scratched or bruised even in the slightest amount, more than half its strength is lost [6]. Fracture of glass originates at small imperfections or flaws, the large majority of which are found at the surface [5]. A bruise or contact with any hard body will produce on the surface of glass very small cracks or checks that may be invisible to the naked eye. Nonetheless, due to their extreme narrowness, they lead to a concentration of stress that may be many times greater than the nominal stress at the section containing them. The applied stress, when it is high enough, causes these flaws to propagate since glass cannot yield [5].

The principal causes of glass container breakage defined by Moody [7] are internal pressure, vertical load, and impact. Impact occurs when a bottle is dropped or bottles impact each other on filling lines. There are many ways of testing glass container secondary packages for adequate protection during normal rail and /or truck shipping and handling conditions. There is not much information available, however, about specific handling and environmental conditions for the secondary packages [8]. Some ways of testing container packages are the Conbur impact test, the bottom drop, and the hydrodynamic drop test. The drop test is used to evaluate the protection available to the bottom of the bottles from the surrounding packaging material [8].

The equipment consists of a drop mechanism, a vertical support that permits changes in dropping height, and a steel plate. The shipping container is placed on the table and the drop leaves are released, permitting the shipping container to fall on to the drop surface.

In this study, the objectives were threefold. The first was to determine the effect of an additional piece of corrugated board below the container as protection against impact by dropping. The second was to determine the effect of viscosity of the contents on the susceptibility to breaking by impact dropping. The last was to determine if the headspace of the contents in containers affects breakage by impact. Also, this work was a demonstration of the use of abraded glass jars to narrow the range of

strength values. By narrowing the range of strength values, more subtle effects on impact breakage can be examined.

EXPERIMENTAL PROCEDURE

Glass Containers

Two designs of soda lime-silicate glass containers were used for this research. One of them was a twenty-eight ounce (800 g) capacity spaghetti sauce jar mold #2803 standard round wide mouth jar with a high shoulder and a 63/203 mm finish packed one dozen per carton (Owens-Illinois, Toledo, Ohio). The second was the quart mayonnaise jar mold #23337/8971037 thirty-two ounce (0.946 l) standard round wide mouth jar with straight sloped shoulders and a 70/470/405 mm finish packed one dozen per carton (Smith Container, Atlanta, Georgia). The caps used for the spaghetti sauce jars were #14922 63/400 mm steel lug cap with safety button closures (Owens-Illinois, Toledo, Ohio). For the mayonnaise jars, #5394 70/400mm steel CT closures were used (Smith Container, Atlanta, Georgia). The spaghetti sauce jars were used in the trials determining the effect of a bottom cushion. The mayonnaise jars were used in the trials determining the effects of viscosity and headspace.

Viscosity Control Solutions

Rhône-Poulenc food ingredient 4500 F® guar gum, a product of India, was used for preparing viscous solutions (Rhône-Poulenc, Cranbury, New Jersey). Two guar gum solutions were prepared to allow a range of viscosity values from water (8.904×10^{-3} poise at 25°C) [9] to honey (420 poise at 25°C) [10]. Honey was chosen as one of the most viscous foods. Three types of solutions were prepared. For the first, plain tap water was put in each jar. For the second, 4 g guar gum + 925 ml hot (estimated between 65 and 82°C) tap water was used and finally, 12 g guar gum + 925 ml hot tap water (estimated between 65°C and 82°C) was utilized. All samples had 5% headspace. On a percentage basis, the guar gum concentrations were 0 for the control, 0.43%, and 1.3%, respectively. The actual measured viscosity values were 8.904×10^{-3} poise for water, 4.14 poise for the intermediate, and 527.07 poise for the high viscosity samples. To make guar gum mix completely with water, a Hamil-

ton Bleach Blend Master Blender (Hamilton Beach/ Proctor-Silex, Inc., Washington, NC) was used at number eight speed with a 350-watt motor providing the power. To measure the viscosity of the guar gum solutions used for imitating viscous foods, a set of Cylindrical Spindles of a Brookfield Viscometer was utilized. Cylindrical spindles provided defined spindle geometry for calculating shear stress and shear rate values as well as viscosity. Before making a viscosity measurement, viscometer model, spindle, rotational speed, container size and sample temperature were recorded. After the gum solutions were blended leaving 5% headspace, each jar was placed under the viscometer by immersing the spindle into the solution. Calculations from the viscometer readings were made according to Anonymous [11].

Corrugated Boxes and Cushions

Two types of secondary packages were used for the two kinds of jars. Trays covered with shrink-wrap were used with the spaghetti sauce jars for the trials determining the effect of a bottom cushion. Regular slotted containers were used in the trials determining the effects of viscosity and headspace. For spaghetti sauce jars, the corners of the trays were taped to help prevent spillage after breakage. The dimensions of the trays were height of 9.21 cm, width of 27.94 cm, and length of 37.15 cm. The weight of the double-faced, single-walled corrugated used for the trays included the innerface of 33 g/m^2 (40.2 lbs/1000ft^2) and the outerface of 34.63 g/m^2 (42.1lbs./1000ft^2). The fluting was of type C with a weight of 28.29 g/m^2 (34.4 lbs./1000ft^2). The cushion used was a sheet of this corrugated board beneath the jars. The dimensions of the cushions placed in the trays were a length of 36.32 cm and width of 27.31 cm. The weight of the double-faced, single wall corrugated cushion included the innerface of 35.53 g/m^2 (43.2 lb/1000ft^2), the outerface of 36.99 g/m^2 (44.97 lb/1000ft^2), and the fluting was of type C with a weight of 31.19 g/m^2 (37.92 lb/1000ft^2). For the mayonnaise jars, the secondary package utilized was a regular slotted container-standard layout with partitions supplied with glassware (Smith Container, Atlanta, Georgia, 1996). The dimensions of the boxes were height of 17.78 cm, width of 31.75 cm and length of 41.66 cm. A standard partition was used to provide separation of mayonnaise jars. The partitions were a set of solid fiber pieces with a 4 × 3 cell arrangement in which the jars were placed. These solid fiber pieces were the full height of the jars. Clearance between glassware

and partitions was sufficient to permit containers to drop readily from cells when the case was inverted.

Preparation of Glass Containers

For all treatments, twenty-eight ounce (800 g) capacity spaghetti sauce jars and thirty-two ounce (0.946 l) capacity quart mayonnaise jars were each abraded by hand using 120 grit (coarse) sandpaper around the circumference of the heel and sidewall. Abrasion is used to narrow the range of strength values of the glass containers. Prior to abrasion with sandpaper, the condition of the surface of each container was determined by the variable treatment of each container during manufacture and handling. By abrading all samples with 120 grit sandpaper, the containers all had essentially the same severity of abrasion. That is, the surface scratches determining strength were all grooves produced by approximately the same size abrasive grains. The radius at the tip of the goove is the strength determining factor, not the overall number of grooves. Hand abrasion is sufficient to produce reproducible weakening provided a specific grit size is used consistently. Overall, abrasion lowers the average strength of a group of containers, primarily by weakening the strongest containers while not weakening those containers that already had 120 grit abrasions from manufacturing and handling. Each jar was then dipped in water, filled, capped by hand and stored overnight. By dipping in water, the variability in glass strength due to differences in exposure to moisture is eliminated. After drying by sitting overnight, spaghetti sauce jars, in-groups of 12, were placed in side slotted trays containing corrugated board bottom cushions. The trays were wrapped in polyethylene film. Next, the film was shrunk to the jars in the trays using a shrink tunnel. In the same way, after filling with tap water or guar gum solution and capping by hand, mayonnaise jars were placed in regular slotted boxes, and then the boxes were taped.

Drop Test

A Gaynes Drop Tester (Gaynes Engineering Co., Chicago, IL) was used for drop tests. The equipment consists of a drop table mechanism; a vertical support permitting changes in drop height, and a steel base plate [12]. A box or tray was positioned on the table, and the drop leaves were released permitting the container to fall onto the drop surface [12]. When

the drop leaves were released, their motion was accelerated with springs so that the leaves did not interfere with a free, unobstructed flat bottom drop. The steel plate below the drop leaves provided a rigid and level dropping surface [12].

Cushion Test

This test was applied only to spaghetti sauce jars. Twenty-four trays without cushions and 24 trays with cushions, each containing 12 spaghetti sauce jars were prepared according to methods above, that is, each jar was filled to 5% headspace with water, capped and thoroughly dried before being placed in the tray. Each tray was shrink wrapped (Heat Sealer, Cleveland, OH), and sent through a heat seal tunnel (Ampack, Hudson, OH) at 350°F for 25 seconds. Two types of secondary packaging were tested in the cushion test: trays without a cushion and trays with a cushion. For the trays with a cushion, each was cut to fit and placed underneath the jars so that the entire base of each jar rested completely on a cushion. The drop tester allowed for each package to be dropped at a measured height directly on to the base platform. If any of the jars broke in the dropped package, the remaining survivors were put aside and never used again, and the broken glass jars and wet corrugated were thrown away. If no glass breakage occurred, it was tested again 5.08 cm higher until breakage occurred. The drop testing began at a height of 15.24 cm. After dropping, all of the broken jars were observed in terms of breakage patterns and locations.

Headspace Test

Three levels of headspace were tested for the second treatment, with mayonnaise jars. After abrasion, jars were filled with water, leaving 10%, 5% and 0% headspace. Each jar was then capped and thoroughly dried. After that, each jar was placed with partitions among jars in a regular slotted container. Twenty-four cases of a dozen jars for each headspace level were taped. Drop tests were conducted as in the cushion test.

Viscosity Test

The controlled viscosity solutions, prepared in mayonnaise jars as de-

scribed above, all were capped, dried and placed in the regular slotted container-standard layout boxes in groups of twelve. Partitions were put among the jars. After that, the boxes were taped and tested as described in the cushion test.

Visual Evaluation

Each case containing one or more broken jars was examined by eye. For the mayonnaise jars, in corrugated boxes, breakage was readily determined by observing the water or solution leaking from the regular slotted boxes. For the trays of spaghetti sauce jars, over wrapped with film, breakage was determined by tapping the top of the jar lids. If breakage had occurred, the tape on the boxes was cut immediately. The number of jars broken at each height, their breakage patterns and breakage locations in the boxes were determined and recorded. To record the breakage patterns of the jars, pictures of broken jars in all cases were taken using a 35 mm Nikon F-3 with 60 mm f/2.8 micro Nikon lens research camera.

Statistical Analysis

SAS/STAT [13] was used to analyze the data. A weighted-least-square analysis of categorical response linear contrasts was used to detect differences between treatment means [14]. In the cushion and the viscosity tests, data were analyzed at a level of significance of 1% ($p < 0.01$) to determine the differences among the treatment means. However, data collected from headspace test were analyzed at a level of significance of 10% ($p < 0.1$) to determine the differences among the sample means.

RESULTS

Effect of Cushion

The cases with no cushion all failed at a height of 30.48 cm or below (Figure 1). Figure 1 shows no breakage for uncushioned samples at heights above 30.48 cm because no uncushioned samples remained unbroken to test at these heights. For cases with a cushion, some survived to a height of 40.64 cm. With the exception of one case that failed at 15.24 cm with a cushion, the range would be 15.24 cm to 30.48 cm for no cush-

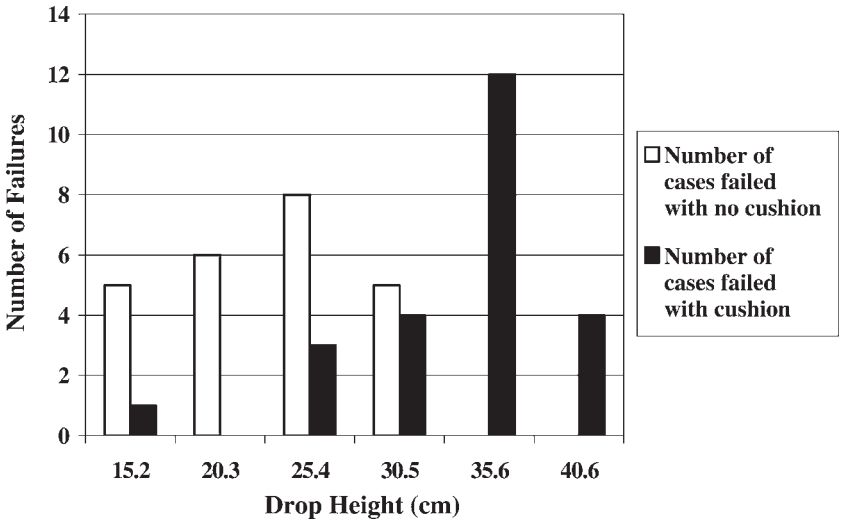

Figure 1. *Case failure with or without Cushion (Twenty-four cases of a dozen spaghetti sauce jars with no cushion and with cushion dropped at each height diminish as cases exhibiting breakage at lower heights are removed from the sample).*

ion and 25.4 cm to 40.64 cm for cases with a cushion. Half of the jars in the cushion treatment broke at 35.56 cm. With no cushion, most of the breakage occurred at 25.4 cm. The percentage of jars that break with or without a cushion increases with drop height (Figure 2). Except for one jar that was broken at 15.24 cm, 25.4 cm would be the drop height where the breakage starts to occur with a cushion. Linear contrasts showed that the effect of using a cushion is to improve breakage resistance, increasing the drop heights needed for breakage ($p < 0.01$) (Table 1).

Effect of Headspace of Contents

The cases whose contents had no headspace all failed at a height of 45.72 cm or less (Figure 3). The cases whose contents had headspace values 5% and 10% all failed at a height of 40.64 cm or less. The range would be 25.4 to 40.64 cm for 10% and 5% headspace cases with the exception one case of 10% headspace that failed at 20.32 cm. The range of 0% headspace cases was from 25.4 to 45.72 cm. Most of the breakage for all headspace cases occurred at a height of 30.48 cm. The percentage of jars that break increases with drop height, except for jars with 5% headspace that showed a dip at a height of 40.64 cm (Figure 4). One jar with 10% headspace broke at 20.32 cm. The effect of using greater

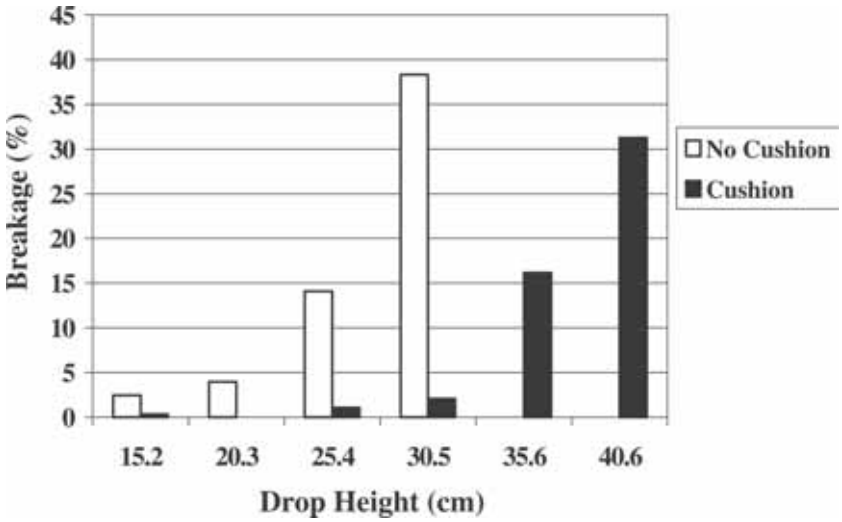

Figure 2. *Breakage as a function of drop height for jars with or without cushion (no. of broken jars/no. jars dropped).*

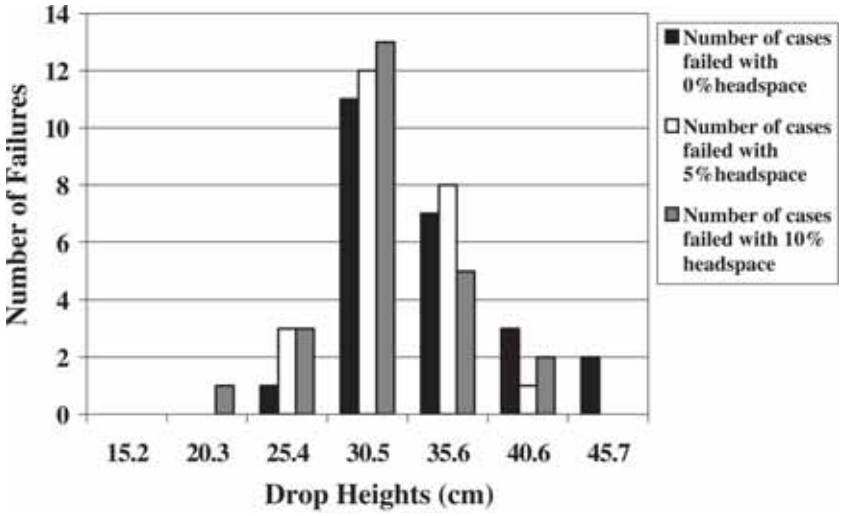

Figure 3. *Case failures with different levels of headspace (Twenty-four cases of a dozen mayonnaise jars for each headspace level dropped at each height diminish as cases exhibiting breakage at lower heights are removed from the sample).*

Table 1. Mean breakage drop heights (cm).

Type of the Cases	Mean ± SE
No Cushion	23.06 ± 1.06[a]
Cushion	33.42 ± 1.16[b]

[a,b]Means with different superscripts are significantly different ($p < 0.01$). Differences between treatments were determined with linear contrasts using a weighted-least square analysis of categorical responses.

headspace is to decrease breakage resistance, lowering the drop heights needed for breakage. 0% headspace cases had a significant difference in mean breakage from 10% headspace cases and 5% headspace cases (p 0.1) (Table 2). 10% headspace cases were not different from 5% headspace (p 0.1).

Effect of Viscosity of Contents

The cases with low and medium viscosity contents all failed at a height of 40.64 cm or less (Figure 5). The ranges for low and medium viscosity cases were from 25.4 to 40.64 cm. High viscosity cases ranged from 30.48 to 55.88 cm. Most of the breakage for low and medium viscosity cases occurred at a height of 30.48 cm. High viscosity cases showed a diffuse peak between 35.56 and 45.72 cm. The percentage of jars that break continuously increases with drop height, except for jars with 5% headspace that showed a dip at a height of 40.64 cm (Figure 6). Breakage begins at a height of 30.48 cm for high viscosity jars, 25.4 cm is the drop height where breakage starts for low and medium viscosity jars. The data for medium and high viscosity jars show the expected steep increase in percentage with increasing height. Low viscosity jars produced a bell shaped curve with a lower percentage breakage at 40.64 than at 35.56cm. The effect of increasing viscosity is to improve break-

Table 2. Mean breakage heights of jars as a function of headspace (cm).

Headspace (%)	Mean ± SE
0	34.29 ± 1.02[a]
5	31.95 ± 0.76[b]
10	31.32 ± 0.91[b]

[a,b]Means with different superscripts are significantly different ($p < 0.1$). Means with the same letter are not different ($p < 0.1$). Differences between treatments were determined with linear contrasts using a weighted-least square analysis of categorical responses.

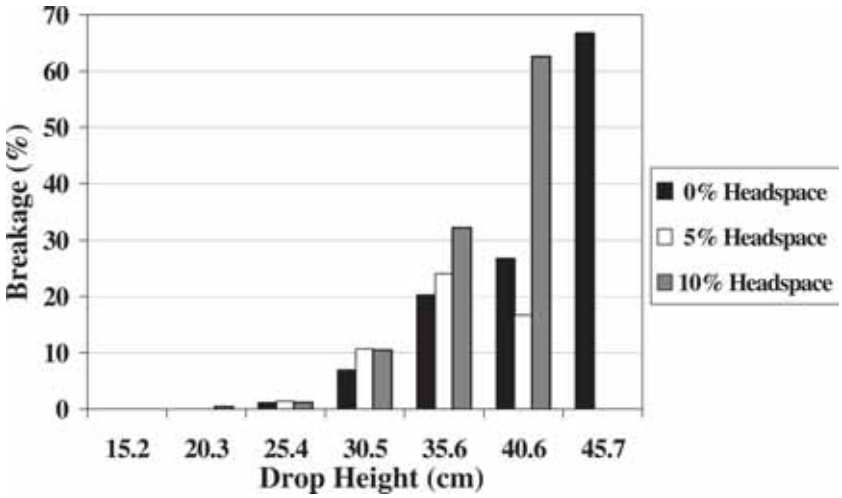

Figure 4. *Breakage as a function of drop height with contents differing in headspace (no. of broken jars/no. of jars dropped).*

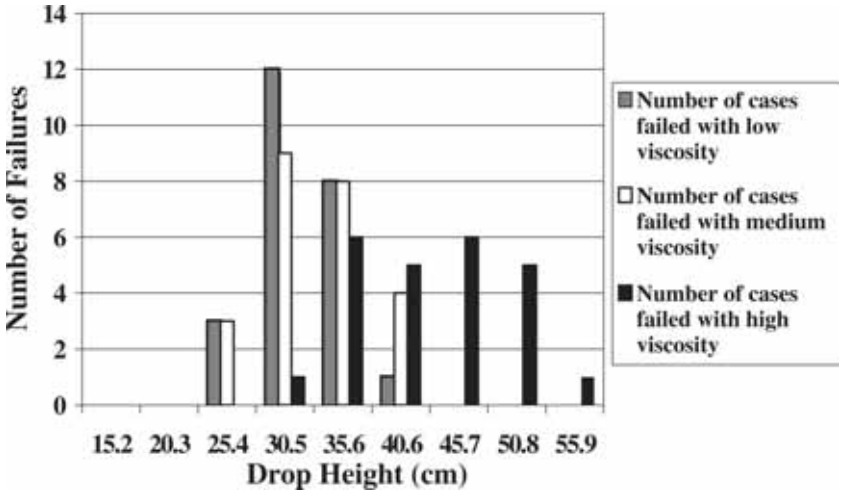

Figure 5. *Case failures with different viscosity levels (Twenty-four cases of a dozen mayonnaise jars for each controlled viscosity solutions dropped at each height diminish as cases exhibiting breakage at lower heights are removed from the sample).*

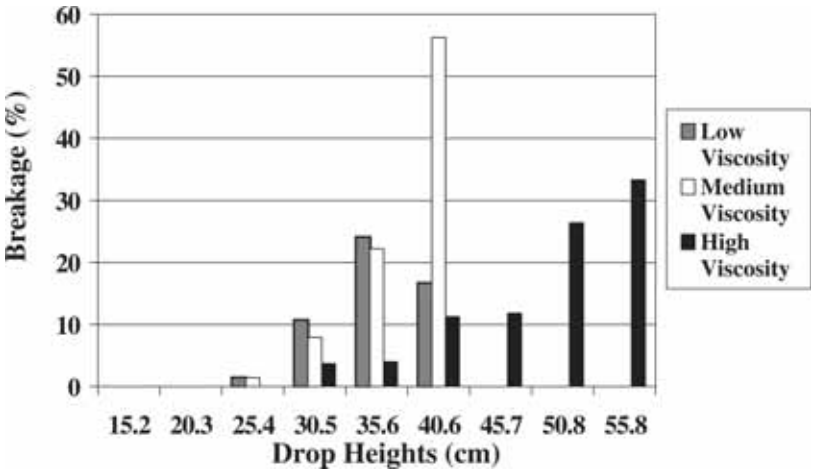

Figure 6. *Breakage as a function of drop height for jars with contents differing in viscosity (no. of broken jars/no. of jars dropped).*

age resistance, increasing the drop height needed for breakage as viscosity is increased. High levels of viscosity cases are different from low viscosity level cases and medium viscosity level cases ($p < 0.01$) (Table 3). However, low viscosity cases are not different from medium viscosity level cases ($p < 0.01$). Mean breakage heights for different levels of viscosity are given in Table 3.

DISCUSSION

The cushion drop test results were as expected. When comparing the cases with a cushion to those without a cushion, using a cushion under the jars provided increased protection against breakage at a 99% level of certainty. It would appear that a small, inexpensive piece of corrugated

Table 3. Mean breakage heights for different levels of viscosity (cm).

Levels of Viscosities (poise)	Mean ± SE
High (527.07)	109.09 ± 0.61^{a}
Medium (4.14)	33.22 ± 0.94^{b}
Low (8.904×10^{-3})	34.29 ± 1.02^{b}

[a,b]Means with different superscripts are significantly different ($p < 0.01$). Means with the same letter are not different ($p < 0.01$). Differences between treatments were determined with linear contrasts using a weighted-least square analysis of categorical responses.

board would be a worthwhile investment in glass container packaging.

The second goal of this research was to determine if different levels of headspace of the contents in containers affect breakage by impact dropping. The results indicate that there was greater breakage at lower drop heights for jars with 5% and 10% headspace than for jars with zero headspace ($p < 0.1$). Also, according to the statistical results, there was a difference in breakage not only between jars with no headspace and jars with 5% headspace but also between jars with no headspace and jars with 10% headspace ($p < 0.1$).

Jars with 10% headspace results were not statistically different from ones with 5% headspace in terms of breakage ($p < 0.1$).

The results for the effect of viscosity of the contents of the jars on breakage by dropping show that high viscosity content jars were less susceptible to breakage than low viscosity or medium viscosity jars ($p < 0.01$). However, low viscosity content jars could not be statistically distinguished from medium viscosity content jars in terms of protection against impact breakage. The results found by testing different levels of viscosity of contents in jars could not be compared with any prior research because no research on this effect has been reported. The tests results concerning viscosity imply that glass containers holding high viscosity foods such as ketchup (187 p at 25°C), mustard (330 p at 25°C), whipped dessert topping (351 p at 25°C) mayonnaise (1000 p at 25°C) will be more resistant to breakage than those containing intermediate viscosity foods such as apple sauce (5 p at 23.8°C) and peach puree (9 p at 26.6°C). These cited viscosity values were measured by Steffe [15].

Breakage Patterns

Observations of the remnants of broken jars revealed breakage patterns consistent with impact breakage origins in the bottom, heel, or lower sidewalls, as expected. According to Knapp et al [16], when the pressure of a liquid in a container is decreased at constant temperature, a state is reached ultimately at which vapor-filled bubbles, or cavities, become visible and grow. The bubble growth may be at a nominal rate if it is by diffusion of dissolved gases into the cavity or merely by expansion of the gas content with pressure reduction. The bubble growth will be "explosive" if it is primarily the result of vaporization into the cavity. This condition is known as cavitation if it is caused by dynamic-pressure reduction at essentially constant temperature. If a growing bubble is sub-

jected to a pressure increase its growth will be arrested and reversed. The bubble will collapse and possibly disappear by solution of gases and condensation of vapor. Collapse occurs "impulsively" for a vapor-filled cavity with negligible gas content and less so if the gas content is high. Cavitation damages containers by removing material from their surface, and it can damage all types of solids including rubber, plastic, glass, quartz, concrete and other nonmetallic solids [16]. For glass containers, cavitation breakage is called hydrodynamic breakage. Of the two thousand three hundred four jars tested in this research, hydrodynamic breakage was observed in just a few jars. The hydrodynamic breakage pattern was typically a small ellipse. In tray-pack tests with or without a cushion, three hydrodynamic breaks occurred in drops from 15.24 and 20.32 cm with water and 5% headspace. In a no cushion case, a small heart shaped breakage area was located in the shoulder of the jar (Figure 7), extending a crack down the sidewall. In a cushion case, there was a loop shaped hydrodynamic breakage on the heel (Figure 8), and also a crack extended up its sidewall.

Another breakage pattern was observed in a jar with no cushion at 15.24 cm height with 5% headspace and water. The pattern appears to be a combination of hydrodynamic and common point source impact

Figure 7. *Hydrodynamic breakage located on the shoulder of jar with no cushion.*

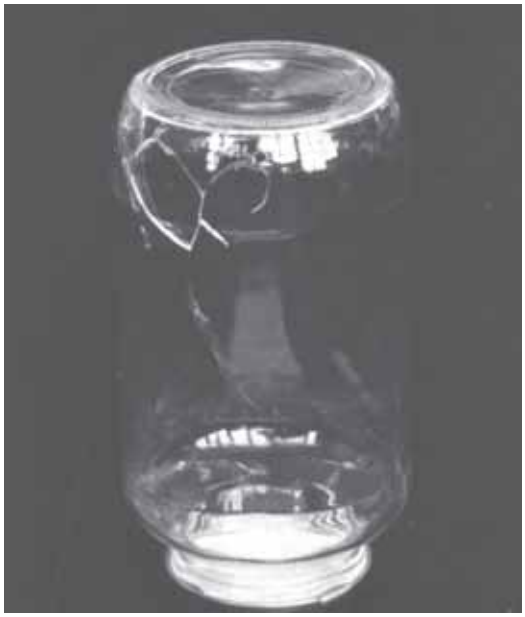

Figure 8. *Hydrodynamic breakage situated on the heel of jar with cushion.*

Figure 9. *An example of a combination of hydrodynamic breakage and normal point source branching.*

breakage. The pattern consists of a large cavity in the bottom that includes part of the heel and sidewall, and branching cracks extending upward (Figure 9). The observation of this pattern in the fracture remnants of one jar suggests that this combination breakage may have occurred in more samples. However, if branching cracks reached further up the sidewall to the neck of a jar, the remnants would not be distinguishable from normal impact breakage.

All three of these jars were filled with water and 5% headspace (Figure 7, 8, and 9). This is contrary to the comments in the literature [6]. Hanlon [6] notes that when containers containing heavy syrups or pureed foods are dropped, hydrodynamic breakage may occur. In this research, no hydrodynamic breakage was observed in the high viscosity samples, or even in the medium viscosity samples. Concerning the increase in breakage susceptibility for jars with 5–10% headspace and for jars with low and medium viscosity contents, the explanations for these effects may be related to the occurrence of cavitation. With 5–10% headspace, bubbles or cavities are more readily formed in the liquid from gases dislodged from above the product due to impact. Similarly, low viscosity liquids would allow more rapid transmission of pressure and possibly more rapid diffusion of dissolved gases out of, then into the liquid. The more rapid onset and end of cavitation might produce greater peak hydrodynamic forces in the glass containers.

In this research, 2,304 glass containers packed in trays or boxes were used. All but two of the jars fit a normal breakage distribution pattern according to breakage heights. However, two jars in the cushion and headspace trials broke outside the normal distribution range. Statistically, they cannot be omitted from the survey although they have little effect on the stated results. In commerce, the two jars that broke at very low drop heights are of critical importance. These are the jars that break on a smooth running filling line or even in properly designed cases. These jars may have had a manufacturing defect, fault, or weakness (e.g. a small bubble in the heel or unmelted piece of sand in the glass) that caused them to be much weaker than the other jars.

CONCLUSIONS

First, there was a statistically significant difference in breakage susceptibility between using a cushion under the jars and using no cushion under the jars at a point $\forall = 0.01$ level of certainty. Cushions provided

increased protection for the trays dropped from a range of heights. This result was expected based on previous studies. Second, when headspace is increased from zero to 5% or 10%, susceptibility to impact breakage increased. An increase from 5% to 10% produced no greater susceptibility to breakage. Jars with no headspace survived to greater drop heights. Finally, the highest viscosity level of contents in jars provided greater protection against breakage. In conclusion, according to the results of this research, glass jars filled with high viscosity foods with no headspace are less susceptible to impact breakage than jars filled with low viscosity foods with a headspace of 5% or 10%. The observed effects may be related to cavitation forces increasing with greater headspace and lower viscosity.

ACKNOWLEDGMENTS

This research was supported by the South Carolina Agricultural Research Station and by the Turkish Ministry of Education. Much appreciation is given to Turkish Ministry of Education, for financially supporting the author Necla Demir during her study. The authors are also grateful to Dr. Robert F. Testin and Dr. Ronald L. Thomas for their collaboration.

REFERENCES

1. Michalske TA, Bunker BC. The fracturing of glass. *Scientific American.* Dalton, MA, 1987; 122–129.
2. Vergano PJ. Glass container. *Ceramics and Glasses, Engineered Materials Handbook.* ASM International the Materials Information Society, 1991;?4: 1084–1086.
3. Boyd DG, Thompson DA. *Glass: Kirk-Othmer Encyclopedia of Chemical Technology.* Wiley-Interscience: New York, 1982; 11:807.
4. Shand EB. *Glass Engineering Handbook.* McGraw-Hill: New York, 1958: 1–47, 197.
5. McLellan GW, Shand EB. *Glass Technology: Glass Engineering Handbook.* McGraw-Hill: New York, 1984; 30–32.
6. Hanlon JF. *Glassware: Handbook of Package Engineering.* Technomic Publishing: Lancaster, 1992; 1–10.
7. Moody BE. *Packaging in glass.* Hutchinson and Benham: London, 1977; 104.
8. LeButt RD. *Laboratory Test Exhibits Rail/Truck Shipping and Handling Guidelines.* Owens-Illinois Forest Products Division: Ohio, 1982.
9. Robert CW. *Viscosity of liquids: Handbook of Chemistry and Physics.* The Chemical Rubber Co.: Ohio, 1968; F-36.
10. Crane E. Honey: *A Comprehensive Survey.* The International Bee Research Association, Heinemann: London, 1976; 219–222.

11. Anonymous. *More solutions to sticky problems: a Guide to Getting More from Your Brookfield Viscometer.* Brookfield Engineering Laboratories: Massachusetts, 1991; 3–24.
12. ASTM. *Standard test method for drop test for loaded boxes (committee d-10) performance testing of shipping containers: American Society for Testing and Materials.* Philadelphia, 1987; 23–25.
13. SAS. SAS/STAT Guide for Personal Computers, Version 8 e. SAS Institute, Cary, NC. 1998.
14. Agresti A. *Weighted least squares for categorical data: Categorical Data Analysis.* Wiley: New York, 2002; 15:1.
15. Steffe JE. *Rehological properties of fluid foods: Data compilation: Physical and Chemical Properties of Food.* ASAE publication, 1986; 210–232
16. Knapp TR, Daily JW, Hammit FG. *Cavitations and cavitations types and effects: Cavitation.* McGraw-Hill: New York, 1970; 1–19.

Development of a Finite Element Model of Pallet Deformation and Compressive Stresses on Packaging within Pallet Loads

JONGKOO HAN[1,*], MARSHALL WHITE[2] and PETER HAMNER[3]
[1]*Assistant Professor, Department of Wood Science & Forest Products, Center for Unit Load Design Virginia Tech, 1650 Ramble Road, Blacksburg, VA 24061*
[2]*Professor, Department of Wood Science & Forest Products, Center for Unit Load Design Virginia Tech, 1650 Ramble Road, Blacksburg, VA 24061*
[3]*Research Associate, Department of Wood Science & Forest Products, Center for Unit Load Design Virginia Tech, 1650 Ramble Road, Blacksburg, VA 24061*

ABSTRACT: Pallets maybe exposed to an exceptional variety of external forces. Distribution of these forces over the pallet deckboard and between the pallet deck and packaging are non-uniform. The static stress distributions across pallet decks were quantitatively characterized when supporting packages. Pallet test sections consisted of one top and one bottom deckboard segment, were made of Plexiglas® instead of wood with two stringer segments. The corrugated fiberboard pad, pressure sensitive film, a series of image processing techniques, and commercial finite element package were introduced to analyze the stress distributions and to develop a mathematical model of the deformation of wood pallet deckboards covered by compressive stresses imposed by packaging.

INTRODUCTION

THE pallet is a pavement that covers the supply chain highway. Modern supply chain systems cannot be readily organized or operated speedily without it. Commercially available computer software for unit loads, such as CAPE™ and TOPS™ concern primarily the geometric "fit" characteristics of unit loads and its components. These programs do not estimate the structural performance of the components of the pallet load. They might not assist unit loads engineers select components and materials that improve the resistance of the unit load to hazards during

*Author to whom correspondence should be addressed. Email: hanjongk@vt.edu

1557-7244/07/03 149-14

materials handling. White & Hamner (2004) demonstrated the stresses are non-uniform and depend on the stiffness of the pallet deck components in their recent study, "Topographical Mapping of the Mechanical Stresses on Wood Pallets during Use." One key element of the development of structural design technologies for unit loads will be predicting the mechanical stresses imposed on the packaging by the pallet deck, as a function of properties of the pallet deck and the properties of the packaging placed on the pallet. It would be the first effort to visualize the static stress distributions and the deformation of wood pallet deckboards. The static stress distributions across pallet decks were quantitatively characterized and a mathematical model was developed using a finite element method (FEM) of the deformation of wood pallet deckboards by compressive stresses imposed by package simulation systems.

The major aim of this research is the development of a predictive mathematical model, using finite element techniques. This initial model will focus on predicting the effect of static compressive stresses which occur between packaging on the pallet deck during unit load stack storage. Such a model will assist pallet, unit load, and package designers select the most efficient combination of components for unit load design when stack storage compressive stresses are limiting. This is a critical step in the solution of the complex problem of the structural design of the entire unit load. The objectives of this research are to:

- Quantitatively characterize the static stress distributions across pallet decks when supporting packages: simulated with corrugated containers.
- Perform a numerical analysis and develop a mathematical model using a finite element method of the deformation of wood pallet deckboards covered by compressive stresses imposed by packaging.

MATERIALS AND METHODS

Preparation of Pallet Samples

Pallet test sections consisted of one top and bottom deckboard segment ($20'' \times 3.5''$, L × W) with deck thicknesses of 3/4″ and two-stringer segments were tested (Refer to Figure 1). Instead of wood, Plexiglas®, an acrylic base plastic material (major physical properties are presented

Figure 1. *Example of pallet test section sample with Plexiglas® deckboard.*

in Table 1) was used as deck board material, since its mechanical properties were more consistent than wood. Oak was selected as a stringer material. Three replicates were made of each of two joint methods. Each specimen was tested twice, so that any data presented in this report is an average of six measurements. Two joint methods between deckboards and stringers were applied; "pin (free movement between the deck and stringer)" and "semi-rigid (nailed joint between the deck and stringer)".

Testing for Characterizing the Static Stress Distributions and Measuring Deformation

A uniform compression load was applied to the pallet samples using an MTS 10 Kip servo-hydraulic universal test machine. A strip of

Table 1. Physical Properties of Plexiglas®.*

	Test Method	Properties	Unit
Specific Gravity	ASTM-D-792	1.19	
Tensile Strength			
Yield	ASTM-D-638	11,250	psi
Elongation		6.4	%
Modulus of Elasticity		450,000	psi
Flexural Strength			
Rupture	ASTM-D-790	15,250	psi
Modulus of Elasticity		475,000	psi
Compression Streng			
Yield	ASTM-D-695	18,000	psi
Modulus of Elasticity		440,000	psi

*Information was provided by SPARTECH POLYCAST Co.

$$p = \begin{cases} 1 - \exp^{-\exp(\beta_n + \beta_1 (Size - \exp^{(c_0 + c_1 Pressure + c_2 Pressure^2)}))} \text{ if } Size - \exp^{(c_0 + c_1 Pressure + c_2 Pressure^2)} \geq 0 \\ \end{cases}$$

Pressurex® film having a low-pressure sensitivity ranging from 2–20 psi was applied to the top deck component of each sample such that it covered the entire top deck surface area. This range of film pressure sensitivity was appropriate since warehouse stack storage of heavy unit loads results in forces of approximately 2 to 6 psi. A layer of single wall C-flute corrugated fiberboard (35–26C-35) was applied over the pressure film to simulate the bottom of a corrugated box. The samples were then tested in compression using a rigid steel tube applicator spanning the length and width of the pallet section. Figure 2 is a photograph of the test setup. Loading was halted after reaching a load consistent with 14–17 psi (approximately 1,000–1,200 lbs) for each pallet section sample. High pressures (compression) were used to generate measurable contrast within the range of the film. The results from this test were recorded using digital photographs or scanners to document similarities and differences in stress distributions between pallet sections.

In this study, the single wall C-flute corrugated fiberboard was applied not only as a simulation of the corrugated box packaging but also as a sensing medium to indicate the static stress. It might be the first effort to apply this material to detect these static stresses.

The deformation of pallet deck board by compressive stresses was measured. String Potentiometers (UniMeasure, Corvallis, OR. USA)

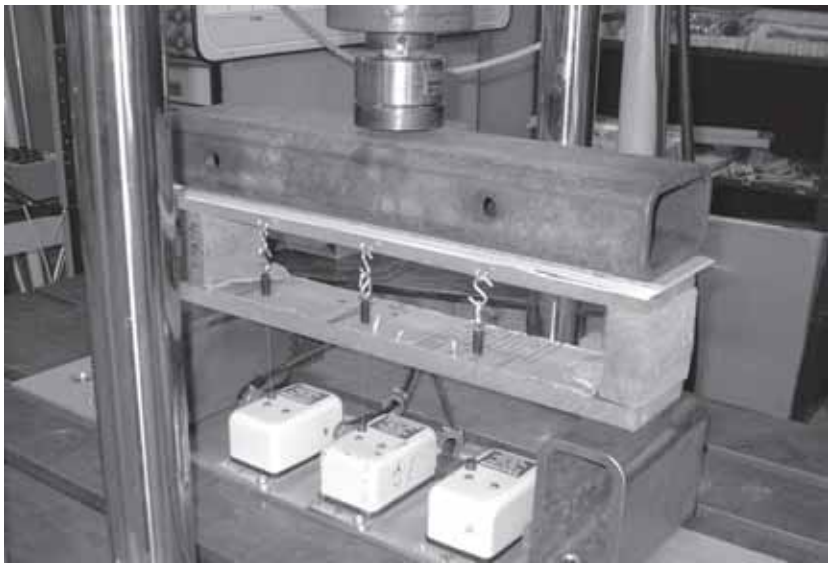

Figure 2. *Testing set-up for pallet sample compression.*

were used to measure the deformation of pallet samples. From the left end of the samples at location of 5″, 10″, and 15″ three string potentiometers were installed and deformation of pallet was recorded automatically.

Modeling

For modeling, a compression load of 14–17 psi (approximately 1000–1200 lbs load on each pallet section sample) was applied and an average of 6 measurements of the maximum deformation was compared with simulation results. A numerical approach using a finite element method was used to model the deformation of wood pallet deckboards by compressive stresses. The commercially available software package ANSYS release 9.0 ED Version was used.

RESULTS AND DISCUSSION

Characterizing the Static Stress Distributions

Even though the corrugated fiberboard pad has some limitation such as inconsistency in paperboard quality, it was found that there might be a great possibility of using it as a sensing medium for detecting static stress. In this study, a C-flute corrugated fiberboard pad was actually used to detect and analyze the static stress and their distributions. Figure 3 is a typical result after compression. The thickness of each stripe, impression by the flute of corrugated fiberboard pad, at each location along a pallet deckboard were measured. The applied pressure at each location along the deckboard is estimated using the standard calibration curve, which was constructed separately. Though the original image data was

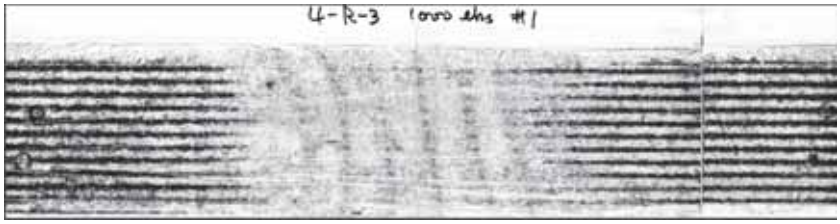

Figure 3. *Image left by medium of corrugated fiberboard on pressure sensitive film between the packaging and pallet deckboard.*

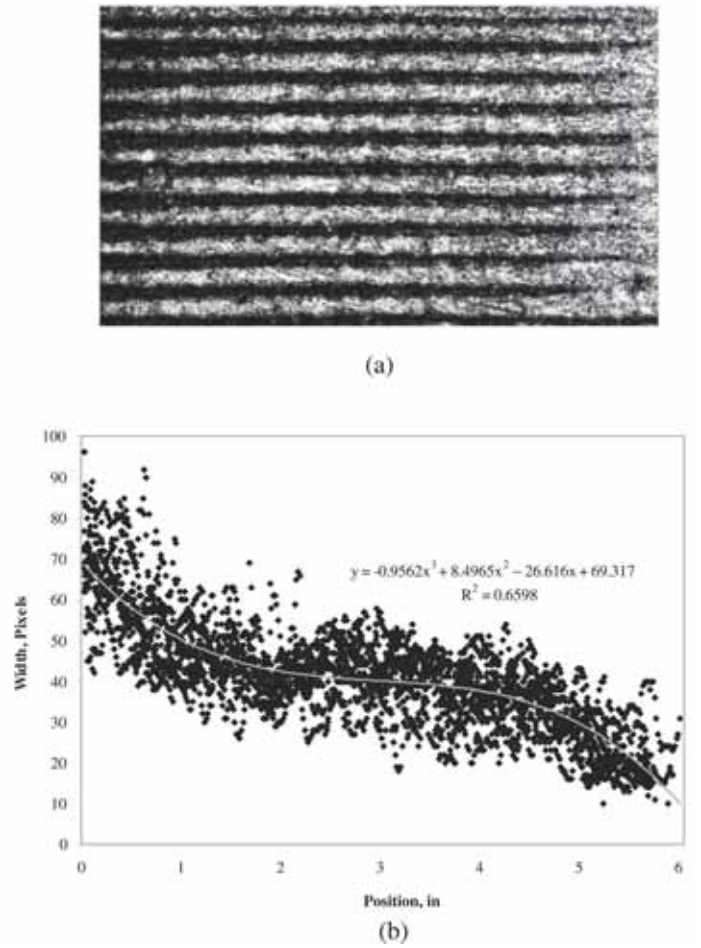

Figure 4. *Thickness of stripe at any location on the deckboard; (a) Original image and filtered edges, (b) 3rd order polynomial regression.*

very "noisy" because of limited resolution, the edges of each image could be filtered and resolution improved [Figure 4 (a)].

Figure 4 shows an example of the application of the calibration curve. Throughout the deckboard, there were mostly 11 stripes at a given location so that 11 thickness values were available at any location along the deckboard length. Figure 4 (b) presents a relationship between the thickness of stripes in pixels and the location on the deckboard. A regression with the 3rd order polynomial was used to analyze the relationship between image thickness and location.

Figure 5 shows the results of compression testing analysis for the pinned and semi-rigid joints. These results were used to model the deformation of the deckboard supporting non-uniformly distributed loads.

Measurement of Deformation

Figure 6 is a plot of maximum deckboard deformation as a function of compression loads applied. There is no relationship. It is estimated that

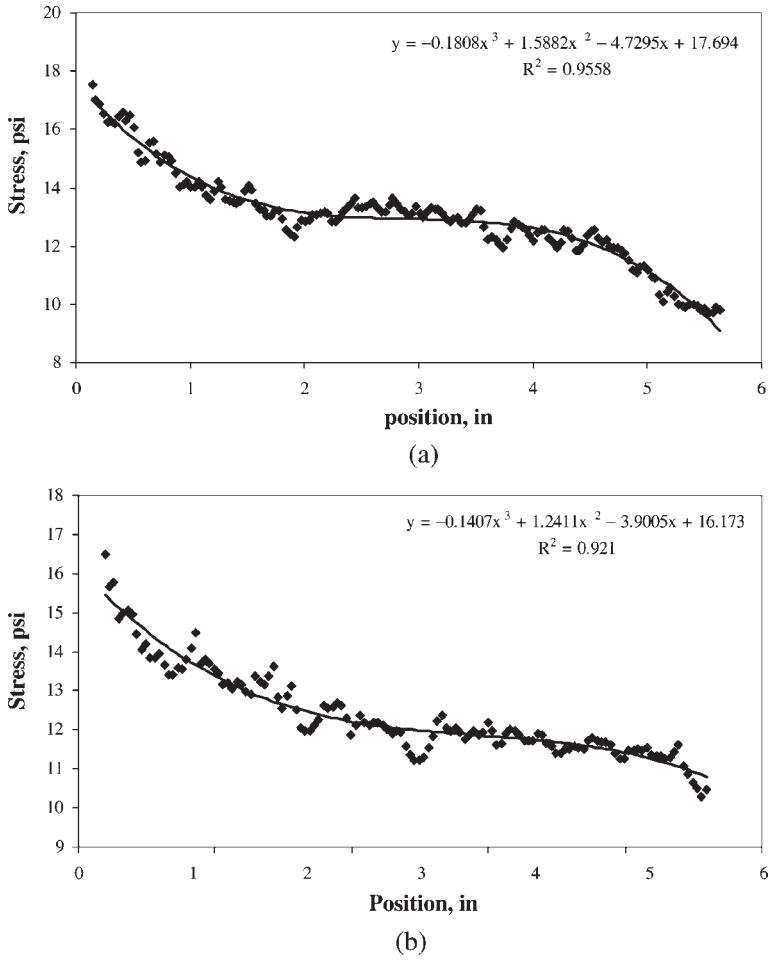

Figure 5. *Relationships between position along deckboard, deckboard stiffness, joint stiffness, and stress applied to the deckboard; (a) Compression test result for pin joint, (b) Compression test result for semi-rigid joint.*

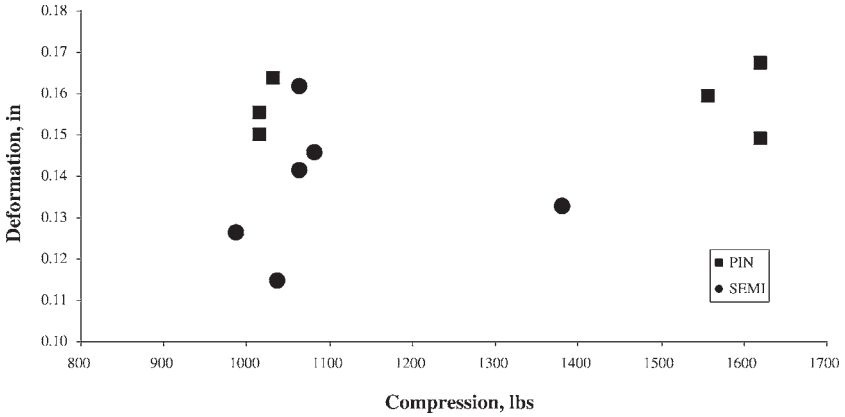

Figure 6. *Maximum deformation of the deckboards vs. compression loads.*

the corrugated fiberboard pad acted as a cushioning material between the steel tube beam and Plexiglas deckboard substitute. The lack of relationship between applied loads and deformation were not unexpected because the loads transferred through the corrugated fiberboard is non-uniformly distributed. Table 2 summarizes the results of the deformation tests and Figure 7 shows these results graphically. As expected, the pallet section with "pin" joint showed larger deformation. Clearly the joint method affects deckboard deformation under load.

Modeling Deformation by a Finite Element Method

The finite element method is a numerical procedure for solving physical problems governed by a differential equation or transient relationships. It can be described as an adaptation of the calculus of variations, and results in a system of simultaneous linear or nonlinear equations.

Table 2. Deformation of deckboard pallet section.

	Distance from the left end of the pallet section, in.				
Joint Method	**1.25***	**5**	**10**	**15**	**18.75***
Pin	0	0.131	0.157	0.112	0
Semi-Rigid	0	0.102	0.137	0.099	0

*1.25″ and 18.75″ represent the inside edge of the stringer.

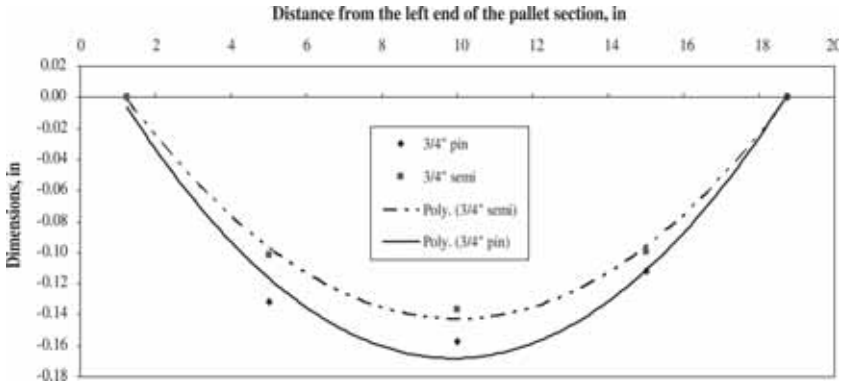

Figure 7. *Graphical Presentation of Deformation of deckboard pallet section.*

The number of equations is usually very large, so the method has practical value only with use of computer technology. The finite element method has two characteristics that distinguish it from other numerical procedures (Segerlind, 1984):

- The method utilizes an integral formulation to generate a system of algebraic equations;
- The method uses continuous piecewise smooth functions for approximating the unknown quantity or quantities.

In this study, a commercially available software package, "ANSYS Release 9.0 ED version" was used to model the deformation of the deckboards of the pallet section samples.

Compression on the pallet section can be modeled as a simple, single load step, structural static analysis of 2-dmensional solid rectangle. The dimension of the pallet sample is 20″ × 3.5″with deckboard thickness of 3/4″. The deckboard of pallet section sample was made of Plexiglas® with a Modulus of Elasticity (MOE) of 4.4×10^5 psi and poisson's ratio of 0.30. "Plane stress" was assumed since the deckboard of pallet system is thin in the y direction.

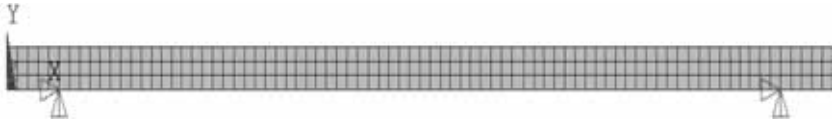

Figure 8. *Front 2D view of the upper pallet deck, with element mesh.*

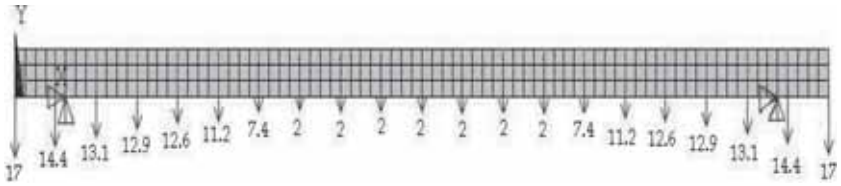

Figure 9. *Modeling example for the pin joint system.*

A two dimensional simple beam, 20″ × 0.75″ was used to model the pallet section deckboard. A 0.25″ × 0.25″ element was adequate to model connection influence. An element mesh was applied to the simple beam. Each square is an element and line crossing is a node in Figure 8. The node numbers are automatically generated by the computer.

Pin Joint Connections

The connections were similarly modeled. In the case of the pin joint, there should be no displacement constraints and the deckboard can freely move vertically except at the inner edge of stringer ($6P^{thP}$ node from both ends). Since each element has a size of 0.25″ and width of stringer is 1.25″, a distance from the end of the deckboard to the inner edge of the stringer is 1.25″ so that the $6P^{thP}$ node from both ends should have 0 displacement (1.25/0.25 = 5). A non-uniformly distributed load can be determined from the regression equation in Figure 5(a) for the pin joint sample. These stresses or load levels are in Table 3 as a function of distance from the end of the deckboard.

The system is modeled and graphically presented in Figure 9. At the $6P^{thP}$ nodes from both ends in Figure 9 for all degrees of freedom, displacement should be 0 (Refer to the triangles in Figure 9). The simulation result is graphically shown in Figure 10. The maximum deformation was 0.152, which agrees well with experimental results, 0.157.

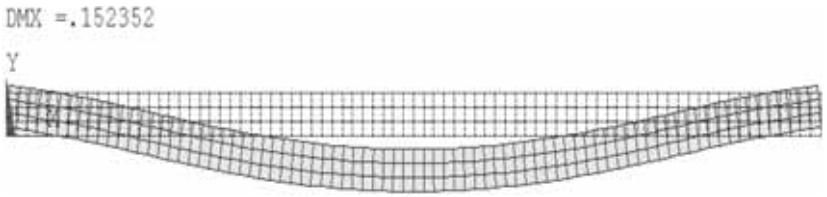

Figure 10. *Simulation results of pin jointed pallet sample.*

Table 3. Non-uniformly distributed loads for the pin joint sample.

Distance from the left end	0	1	2	3	4	5	6	7*	8*	9*	10*	11*	12*	13*	14	15	16	17	18	19	20
Load, psi**	17	14.4	13.1	12.9	12.6	11.2	7.4	2	2	2	2	2	2	2	7.4	11.2	12.6	12.9	13.1	14.4	17

*For between 7″ to 13″ from the left end of the deckboard, 2 psi of loads were assigned for each nodes considering the detection limit of the pressure sensitive tape, which was 2 psi.
**Load = pound/3.5″/20″: Modeled as loads were distributed for every 1″ of deck surface.

Table 4. Non-uniformly distributed loads for the 3/4″ deckboard pin joint sample.

Distance from the left end	0	1	2	3	4	5	6	7*	8*	9*	10*	11*	12*	13*	14	15	16	17	18	19	20
Load, psi**	17	13.4	12.2	11.8	11.4	10.1	7.1	2	2	2	2	2	2	2	7.1	10.1	11.4	11.8	12.2	13.4	17

*For between 7″ to 13″ from the left end of the deckboard, 2 psi of loads were assigned for each nodes considering the detection limit of the pressure sensitive tape, which was 2 psi.
**Load = pound/3.5″/20″: Modeled as loads were distributed for every 1″ of deck surface.

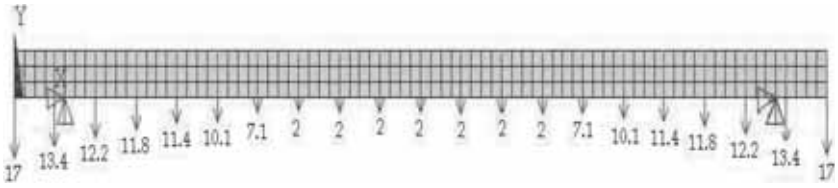

Figure 11. *Modeling for the semi-rigid joint system of simulating the connection stiffness.*

Semi-Rigid Joint Connections

Two methods can be used for modeling the semi-rigid joint connections. First, non-uniformly distributed loads can be determined from the regression equation in Figure 5 (b). These are shown in Table 4. The system is modeled and graphically presented in Figure 11. Again at the 6P^{thP} nodes from both ends in Figure 11 for all degrees of freedom, the displacement should be 0. Simulation results indicate that the maximum deformation was 0.139, which agrees well with experimental results, 0.137.

The other method of simulating the connection stiffness is to apply a constraint to the movement of the nail itself. Since an average distance from the end of the deckboard and the location of nailing was approximately 0.5″ (node No. 4 from the left of the deckboard: See Figure 12), the deformation at node No. 4 can be used for modeling a "semi-rigid" system.

As the predicted deformation of the deckboard at node No. 4 for pin joint (totally free movement) is 0.01299″ (refer to Table 5 and Figure 12) and a theoretically rigid joint should have 0 displacement. It can be reasonably assumed that displacement of the semi-rigid joint is simply the median point between 0 and 0.01299″, which is 0.00650″.

At node No. 7 from Figure 12, for all degrees of freedom, displacement should be 0, but this case node No. 4 should have a displacement constraint of 0.0065″ in the Uy direction. The maximum deckboard deformation by the computer simulation was 0.122″, which is somewhat

Table 5. Deformation by nodes for pin joint system (free movement).

Node	1	3	4	5	6	7	8
Uy	0.02164	0.01732	**0.01299**	0.00864	0.00418	0.00000	–0.00512

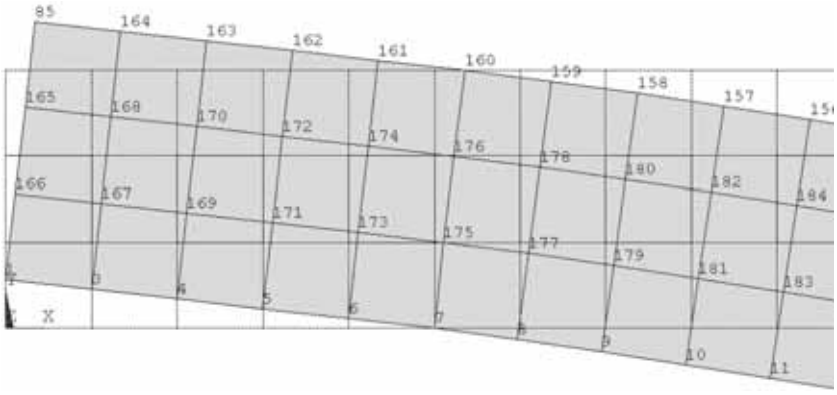

Figure 12. *Enlargement of Figure 10 with node numbers—the left end of the deck.*

underestimates the actual testing result of 0.137″. An appropriate value should be determined from actual experimental measurement in the next stage of this project. However, for this case about 75% of free movement, or a constraint of 0.0098″, would be appropriate, and generates 0.139" of the estimated maximum deformation.

Table 6 shows the comparison of the maximum deformation between modeling by ANSYS and the actual test results. As a sensing medium, corrugated fiberboard worked reasonable well in this study; however, more consistency and higher resolution is needed. A stronger pad such as A-flute or 100% virgin pulp medium C-flute pad might be a better choice.

CONCLUSION

Pallets maybe exposed to a wide variety of external forces. The distribution of these forces over the pallet deckboard and between the pallet deck and packaging are non-uniform.

Corrugated fiberboard pads, pressure sensitive film, a series of image

Table 6. Comparison of maximum pallet deckboard deformation between actual and simulation.

Joint Method	Actual tests, in.	Predicted by ANSYS, in.
Pin	0.157	0.152
Semi-Rigid	0.137	0.139

processing techniques, and commercial finite element package were introduced in this study to characterize the static stress distributions across pallet decks quantitatively and the deformation of the deckboards numerically. This research confirmed that the FEM numerical analysis and the pressure sensitive films can be useful in helping pallet and packaging designers improve the function and efficiency of unit load designs.

Recommendation for Further Research

- More study is needed using pressure sensitive film and corrugated fiberboard pads to quantify stress distributions on pallet deckboards as a function of load and packaging characteristics, materials handling equipment, and pallet deckboard stiffness.
- The finite element method is a powerful tool to model the deformation of wood pallet deckboards under compressive stresses imposed by packaging of different stiffness levels; however, models of the connections between deckboards and stringers need further development.
- Finally, this study should be expanded to characterize the static stress distributions and the deformation across pallet decks when supporting various product and packaging shapes and stacking patterns in the unit load systems.

ACKNOWLEMENT

The authors gratefully acknowledge the funding support for this research project by the Pallet Foundation, Arlington, Virginia.

REFERENCES

1. White, M. and Hamner, M. (2004), “Topographical Mapping of the Mechanical Stresses on Wood Pallets During Use”, Virginia Tech, Blacksburg, VA.
2. Segerlind, L.J. (1984). Applied Finite Element Analysis, 2nd edition, John Wiley & Sons, Inc., New York.

Antimicrobial Packaging: Inactivation Kinetics and Release Modes

PAUL TAKHISTOV
Department of Food Science, Rutgers, The State University of New Jersey, 08901 USA

ABSTRACT: Antimicrobial packaging is a key component of food safety. An antimicrobial agent can be added to a packaging material during film formation, or applied to the food contact surface, which determines different types of antimicrobial packaging materials and antimicrobial release modes. In this work, different modes of antimicrobial agent release have been studied theoretically. A model is developed based on analyses of bacterial populations in response to the addition of an antimicrobial agent as a function of the agent release mode. This model provides a direct connection between microbial inhibition in the food system and the release rate of the antimicrobial agent, and it can be used to design more effective controlled-release packaging materials that will improve the microbiological safety and quality of food products.

INTRODUCTION

RECENT developments in active packaging (AP) have created effective method for preventing bacterial infection [1]. The AP system is designed with antimicrobial compounds to inactivate microbes and prolong the shelf-life of the packaged foods by extending the lag period of the bacterial life cycle and retarding the growth of microorganisms. Antimicrobial packaging is a key component of food safety; it constantly changes with the current needs of the consumers and food manufacturers.

AP provides unique means for allowing controlled release of an antimicrobial agent (AMA). The scope of antimicrobial packaging is very broad and has significant potential to improve the overall food safety system. To facilitate commercial applications of antimicrobial packaging materials, research needs to focus beyond basic feasibility testing and understand the release kinetics of antimicrobial agents from

*Author to whom correspondence should be addressed. Email: Takhistov@aesop.rutgers.edu

1557-7244/07/03 163-17

polymer films and transmittal to the food surfaces. This data need to be coupled with the information about the optimum dose of AMA and methods of specific antimicrobial agents delivery. The main technical challenge is to predict and control the optimal release rate and dose of antimicrobial agent delivered from the active package.

Although a large number of published experimental works describe the kinetics of the microbial inactivation due to the slow release of AMA, there have been no theoretical models developed that can account for the inhibition kinetics, allow predicting of the behavior of the microbial population, distinguish the most appropriate antimicrobial agents and estimate shelf-life of the food product.

THEORETICAL ANALYSIS OF BACTERIA INACTIVATION KINETICS

Controlled Release Modes of an Antimicrobial Agent

An AMA can be added to a packaging material during film formation, or applied to the food contact surface, which determines two major classes of AP materials: releasing and non-releasing films. An antimicrobial releasing film has AMA incorporated into the packaging polymer film, and this agent can migrate to the food surface and inhibit microbial growth. On the other hand, an antimicrobial non-releasing film has an AMA immobilized on the food contact surface and is the site where antimicrobial control occurs.

Generally, AMA's can be delivered to food from AP or added in the food formulation (as depicted in Figure 1). Both non-releasing film with antimicrobial coating and AMA added to the food formulation can be described as a step-like addition of antimicrobial to the bacterial culture. In this paper, these modes of AMA delivery will be referred to as "instant addition" modes. In AP materials with the continuous release of an AMA, the AMA diffuses through the package film and becomes absorbed by the food in direct contact between the product and the film surface. Depending on the properties of the packaging material, the AMA release process can either be steady state or non-steady state. Finally, it is possible for packaging to feature multimodal AMA delivery methods, i.e. the combination of instant AMA addition and its continuous release.

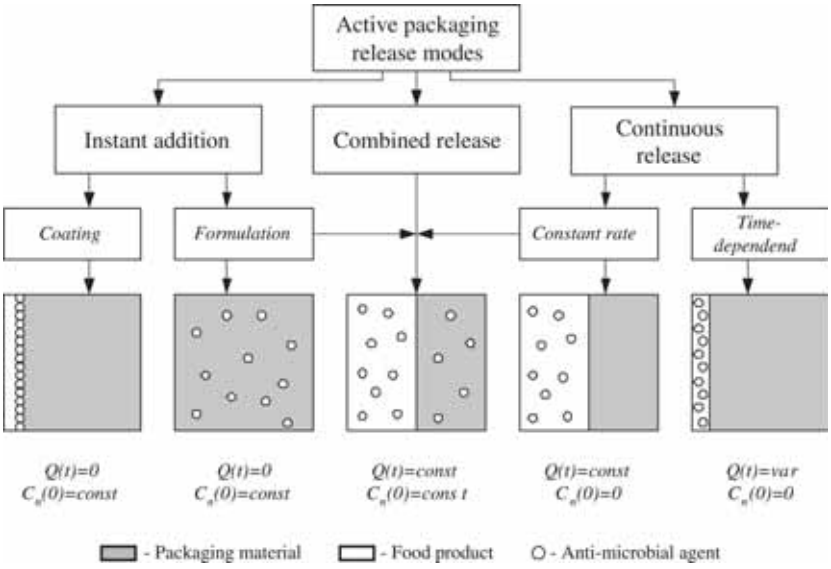

Figure 1. *Schematics of an AP system and the corresponding AMA delivery modes.*

AMA release can be characterized by the following kinetics:

$$\frac{dC_n}{dt} = Q(t) \tag{1}$$

with an initial condition $C_n\big|_{t=0} = C_{n0}$. The release rate $Q(t)$ of an AMA from the AP material is defined as:

$$Q(t) = \frac{d}{dt} M_n(t) \tag{2}$$

where $M_n(t)$ is the amount of AMA released from the packaging material.

The microbial inhibition kinetics corresponding to the AMA delivery scenarios described above can be represented by one of the following AP schemes (see Figure 1):

- AMA is instantly added to a food product (from coating or in formulation);
- antimicrobial agent is continuously added to the product over time;

- the bacterial population is exposed to a combination of the first two strategies;
- AMA is released from the packaging material with limited AMA load capacity.

Model System

The following model can be applied to a variety of packaging materials, AMA's, and target microorganisms. Specifically, we will use Nisin as the model AMA and *Listeria monocytogenes* as the representative microorganism. *L. monocytogenes,* Scott A is a widespread and virulent foodborne pathogen of great concern that can adapt to, survive in, and multiply in extreme environments. It can also survive long periods of drying and freezing followed by thawing [2]. In humans, *L. monocytogenes* causes epidemic and sporadic listeriosis. *Listeria* is one of three major pathogens (including *Salmonella* and *Toxoplasma*) responsible for 1,500 food-related deaths in the USA each year [3].

Nisin (bacteriocin produced by *Lactococcus lactis*) has been shown to be an excellent candidate for use in antimicrobial-releasing films. It has been successfully incorporated into various edible films, polyolefin-based films, and film coatings [4–9]. Nisin alone is effective against gram-positive bacteria and is able to inhibit gram-negative bacteria with the aid of a chelator such as EDTA [10].

Bacterial Kinetics

AP protects foods by inhibiting microbial growth in the food products. Initial bacterial contamination levels in food products are usually very low [11], and can be described initially by exponential growth kinetics:

$$\frac{dC_c}{dt} = \mu C_c \tag{3}$$

The microbial population dynamics in the presence of an AMA released from an AP system and/or added to a formulation is the result of two competitive processes: population growth and inactivation. One of the most frequently used models for inactivation kinetics is the well-known Chick-Watson first-order kinetic model [12]:

$$\frac{dC_c}{dt} = -K_n C_n \tag{4}$$

where: C_c—microorganism population at time t, C_{c0}—initial microorganism population at $t = 0$; C_n = antimicrobial agent residual, K_n—reaction rate.

Combining (3) and (4), one obtains an overall change of microbial concentration in time:

$$\frac{dC_c}{dt} = \mu C_c - K_n C_n \tag{5}$$

The concentration of AMA changes with time due to its release (Equation (1)) and to its reaction with the bacteria (adsorption on the cell wall and/or penetration into the cells) that can be written as:

$$\frac{dC_n}{dt} = -\frac{K_n}{\gamma} C_n + F_n(t) \tag{6}$$

where γ is the antimicrobial agent efficacy factor, i.e. the amount of AMA required to inactivate a certain number of bacteria.

The model approach described so far does not take into account the diffusion/transport of AMA from the packaging material to the food surface. Therefore, this model can be applied for packaged products where the package is in direct contact with the food surface (e.g., RTE meats), or with the thin liquid-filled headspace (hot dogs). The diffusion transport of AMA agent would not influence bacterial inactivation kinetics when diffusion time of AMA migration from the package to the food surface (t_{dif}) satisfies the following condition:

$$t_{dif} << \frac{1}{\mu} \tag{7}$$

where μ is the specific rate of bacteria growth.

Therefore, the critical distance between the package and a surface to be decontaminated can be determined as following:

$$x << \sqrt{\frac{D}{\mu}} \tag{8}$$

where D is the diffusion coefficient of AMA in the food product. Calculations performed for the *L. monocytogenes*/nisin system (bacterium doubling time is 18 min [13], molecular weight of nisin is 3.5 kDa [14])

indicate that the size of headspace should not exceed 100 μm to avoid diffusion limitations for AMA transport. Additionally, AP is deemed to be effective against bacterial contamination when the number of microorganisms during the product shelf life does not exceed its initial value:

$$C_c\big|_{t\to\infty} \le C_{c0} \tag{9}$$

Listeria Monocytogenes Inhibition Kinetics at Various Nisin Release Modes

Bacterial inactivation kinetic model describes the resulting process of exponential bacterial growth and inhibition due to AMA addition with different rates of nisin release and various initial concentrations.

Instant Addition of AMA

As mentioned earlier, AMA can be added to the food product at the time of preparation as a part of the product formulation in order to successfully inhibit bacterial contamination and to decrease the bacterial population to zero. In this case, the spoilage bacteria are exposed to the AMA and there are no other sources of AMA in the system. Therefore, the initial conditions for the system , are the following:

$$C_{n0} = \text{const}; \quad Q(t) = 0 \tag{10}$$

where C_{n0} is the initial concentration of AMA added to the food product by formulation.

Now solving the system (5), (6), one can obtain an analytical solution for the changes in the microbial population as a function of the inoculum (spoilage) size, specific growth rate (μ), inactivation rate constant, and time:

$$C_c = \left[\frac{C_{c0}(K_n\gamma + \mu) - K_n C_{n0} + K_n C_{n0} e^{-(K_n\gamma+\mu)t}}{K_n\gamma + \mu} \right] \tag{11}$$

The concentration of AMA decreases in time according to first-order kinetics:

$$C_n = C_{n0} e^{-K_n\gamma t} \tag{12}$$

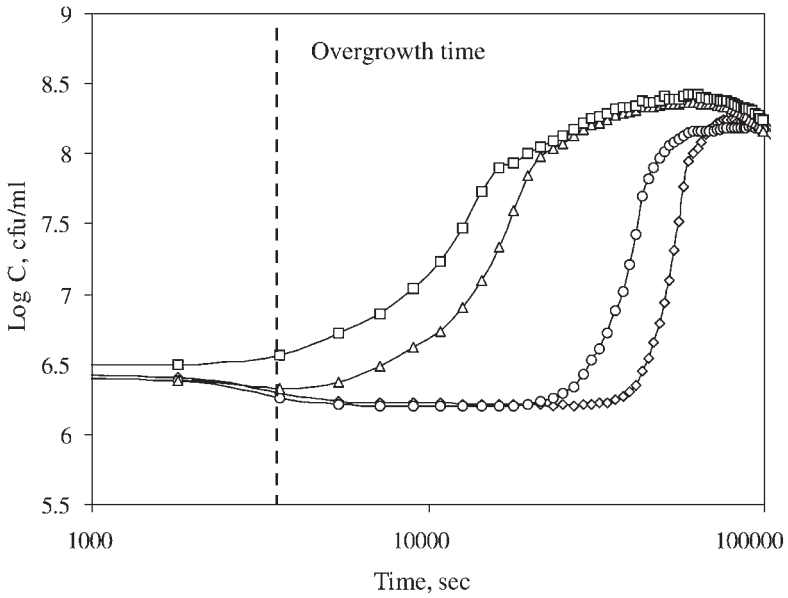

Figure 2. L. monocytogenes *growth in the presence of instantly added nisin:* C_{n0} *= 0, 750, 1000, 2000 IU/mL.*

where C_{c0} is the initial concentration of bacteria, i.e. the size of inoculum (level of bacterial contamination) from which the food product should be protected. Figure 3 depicts experimentally obtained growth kinetics of *L. monocytogenes* at various initial concentrations of nisin.

In comparison, Figure 3 represents the results of numeric calculations, based on the developed model (11). The parameters used in the model are the following: $C_{c0} = 10^5$ cfu/mL, K_n =20, $\gamma = 0.01$. The bacterial kinetics obtained from the calculations is similar to those observed experimentally. Despite its simplicity, the model can qualitatively simulate the bacterial population dynamics.

As we can see that both experimental data (Figure 2) and theoretical model (Figure 3) show the same "overgrowth time"—the time when bacterial population will reach initial (before-treatment) level. This period of time will actually determine the shelf life of the food product.

Analysis of the solution (11) shows that it is possible to find a set of system parameters where the bacterial population would diminish. The expression in the square brackets in equation (11) consists of three terms, the last of which becomes zero at large times. The level of bacterial contamination becomes negligible only if the difference between the

first two terms approaches zero. Solving the equation, one can determine the amount of AMA (C_{n0}) that is necessary to successfully prevent bacterial spoilage with a characteristic growth rate and inactivation kinetics:

$$\frac{C_{n0}K_n}{\gamma K_n + \mu} \geq C_{c0} \tag{13}$$

The inequality in equation (13) reflects the fact that bacteria with higher growth rates require higher levels of AMA initially added to the product. This AMA delivery strategy is the traditional approach for maintaining food safety by modifying the product formulation.

Continuous Addition of AMA at a Constant Rate

The model's representation of AP system includes the continuous addition of AMA's into the product at a constant rate (Q) during its shelf life. This delivery strategy is not used in actual packaging materials, but

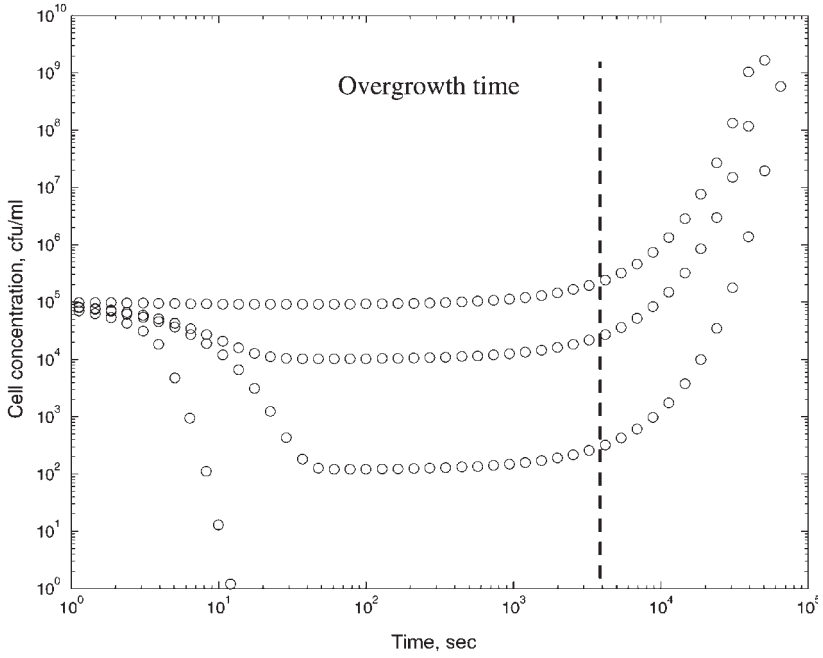

Figure 3. L. monocytogenes *growth in the presence of instantly added nisin: experimental data (a) and numerical simulation results (b).* C_{n0} *= 100, 750, 1000,1500 IU/mL.*

has been experimentally investigated in [15]. The initial conditions for this case are the following:

$$C_{n0} = 0; \quad Q(t) = Q = \text{const} \tag{14}$$

The continuous addition of AMA significantly changes the inactivation process and bacterial population dynamics, as can be seen from the solution of the system (equations (5) and (6)), with the initial conditions (14):

$$C_c = \left[\frac{Q}{\gamma\mu} e^{-\mu t} - \frac{\mu Q}{K_n\gamma + \mu} e^{-(K_n\gamma+\mu)t} + \frac{\mu C_{c0}(K_n\gamma + \mu) - K_n Q}{\mu(K_n\gamma + \mu)} \right] e^{\mu t} \tag{15}$$

The population dynamics depends on bacterial kinetics and on the antimicrobial flux Q (i.e. the material properties of the AP). The corresponding change in the AMA concentration is:

$$C_n = \frac{Q}{K_n\gamma}(1 - e^{-K_n\gamma t}) \tag{16}$$

The results of numeric simulations of *L. monocytogenes* population dynamics as a function of nisin release rate are depicted in Figure 4. It is clear that the continuous addition of AMA is very effective method to inhibit/prevent bacterial population growth. Our results are in good qualitative agreement with the published data [15]. However, this method of AMA delivery is better suited for more long-term applications, and less effective for immediate inactivation of the bacteria.

The concentration of AMA is not a simple decay, but also depends on the AMA flux. The analysis of the system parameters needed to uphold microbial safety of the food product in this case results in an inequality that shows that the continuous addition of the AMA will reduce the bacterial population to zero only for certain values of the AMA delivery rate:

$$\frac{K_n Q}{\mu(K_n\gamma + \mu)} \geq C_{c0} \tag{17}$$

Multimodal AMA Delivery

Chi-Zhang *et al* [15] have shown that microbial population dynamics depends on the mode of antimicrobial agent delivery. The initial addition

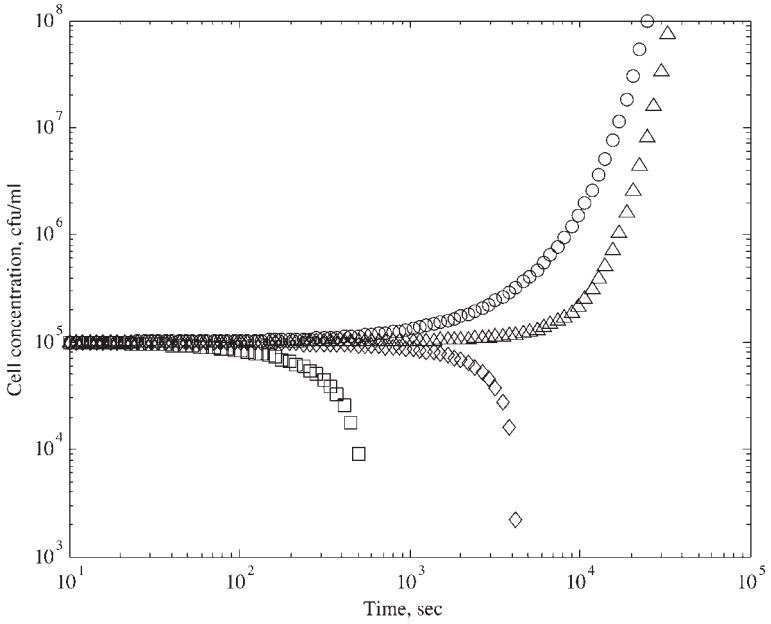

Figure 4. *Calculated* L. monocytogenes *population dynamics as a function of nisin release rate.*

of an AMA is very effective in the early stages of bacterial population development, and the continuous addition method works better for longer times, and seems more appropriate for products with an extended shelf life. In addition, the authors mentioned the synergistic effect of combining the instant (initial) addition and the continuous release modes on *L. monocytogenes* inhibition. The initial conditions in this case reflect changes in the mode of antimicrobial delivery:

$$C_{n0} = \text{const}; \quad Q(t) = (Q) = \text{const} \tag{18}$$

The solution of the system is complex and allows more flexibility in choosing strategies of bacterial population control:

$$C_c = \left[\frac{Q}{\mu\gamma} e^{-\mu t} + \frac{(C_{n0} K_n \gamma - Q)}{\gamma(K_n \gamma + \mu)} e^{-(K_n\gamma+\mu)t} + \frac{\mu C_{c0}(K_n\gamma + \mu) - K_n(Q + \mu C_{n0})}{\mu(K_n\gamma + \mu)} \right] e^{\mu t} \tag{19}$$

The corresponding changes in the AMA concentration can be expressed as follows:

$$C_n = \frac{Q + (C_{n0} K_n \gamma - Q)}{K_n \gamma} e^{-K_n \gamma t} \tag{20}$$

Bacterial kinetics obtained as a result of this model is similar to those depicted in Figure 3 and Figure 4. The combined release mode is more flexible and allows more effective inhibition of the microorganisms. The condition that allows successful suppression of growth and/or inactivation of bacteria can be expressed as:

$$\frac{K_n(\mu C_{n0} + Q)}{\mu(K_n \gamma + \mu)} \geq C_{c0} \tag{21}$$

Time-Dependent Release Rate of AMA

Understanding the release dynamics of the AMA is key in the design of antimicrobial-releasing films and packaging. Due to the finite thickness of AP layers and its limited capacity, traditional AP materials cannot release antimicrobials at a constant rate during the product shelf life period. Upon initial contact with the food product, the AP has a very low AMA release rate, because the polymer matrix is dry and the internal pores of the material are blocked. During the first minutes/hours of contact with the product, the AP material swells due to hydration, pores open, and the AMA release rate increases to its maximum value. After reaching its maximum value, the AMA release rate declines, as the AMA content of the packaging gradually decreases due to the limited amount of AMA that can be embedded into the polymer matrix.

Numerous published data on nisin-based control release films are presented in different ways and very difficult to compare. However, using equation (2) it is possible to obtain normalized data for the nisin release rate as a function of time for various materials. Data on nisin release dynamics collected from the literature are combined in Figure 5.

The bacterial population dynamics is described by the expression (5) as discussed above. As follows from the data in Figure 5, time dependence of AMA release rate can be adequately represented by an exponential function of time ($Q(t) = Qe^{-\lambda t}$) with the exponent factor ($-\lambda$) determined by transport properties of the packaging material. Now the equation (6) with new time-dependent AMA release function from the packaging material can be written as:

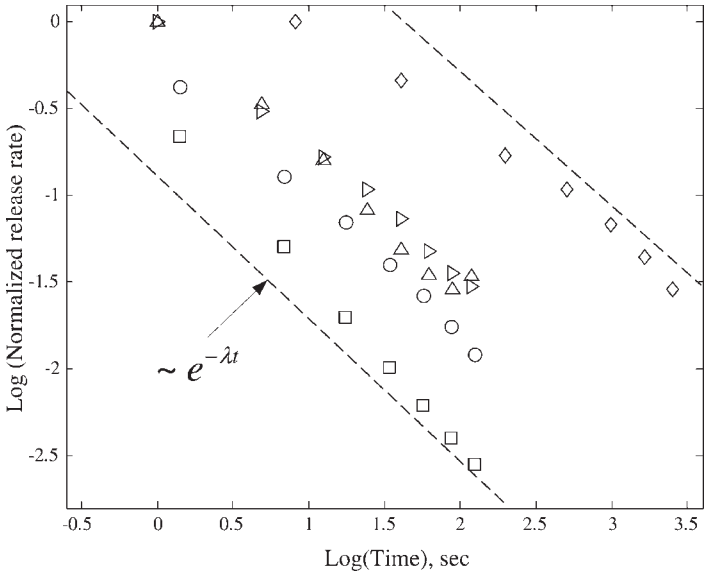

Figure 5. *Time dependence of the nisin release rate from various active packaging materials: films containing 2% (○) and 7% (□) of glyoxal PVOH [16]; (◇)—acrylic polymer film [17]; (△)—acrylic polymer film with 5% nisin [18]; (▷)—vinyl acetate-ethylene co-polymer with 5% nisin [18].*

$$\frac{dC_n}{dt} = -K_n C_n + Qe^{-\lambda t} \tag{22}$$

where $\lambda = f(M_{n0}, h, D_{ns}, D_{nl}, d)$ is the measure of AP efficacy. It is the function of diffusion coefficients of the AMA in the packaging material (D_{ns}) and food (D_{nl}), M_{n0}—the AP material storage capacity, h—mass-transfer coefficient, and d—the thickness of the packaging material.

The solution of the system (5) and (22) is the following:

a) Change of bacterial contamination with time:

$$C_c = \{K_n(K_n\gamma + \mu)Qe^{-(\mu+\lambda)t} + (\mu+\lambda)[C_{n0}(K_n\gamma - \lambda) - Q]e^{-(K_n\gamma+\mu)t}$$

$$+(K_n\gamma - \lambda)\{K_nQ + (\mu+\lambda)[C_{n0}K_n - C_{c0}(K_n\gamma + \mu)]\}\} \tag{23}$$

$$\times \frac{e^{\mu t}}{(K_n\gamma - \lambda)(\mu+\lambda)(K_n\gamma + \mu)}$$

b) Corresponding change of AMA concentration:

$$C_n = \{Q[1 - e^{-(K_n\gamma - \lambda)t}] - C_{n0}(K_n\gamma - \lambda)\}\frac{e^{-K_n\gamma t}}{K_n\gamma - \lambda} \qquad (24)$$

The microbial kinetics in this case is controlled not only by the bacterial inactivation rate constant and growth kinetics, but also by the material properties of the AP. Rearranging (23) one obtains condition for successful protection of the food product in case of time-dependent AMA release from the AP material:

$$\frac{K_n[(\mu + \lambda)C_{n0} + Q]}{(K_n\gamma + \mu)(\mu + \lambda)} \geq C_{c0} \qquad (25)$$

The results of numerical simulation of *Listeria monocytogenes* inhibition by nisin released at various rates from an AP system are depicted in Figure 6.

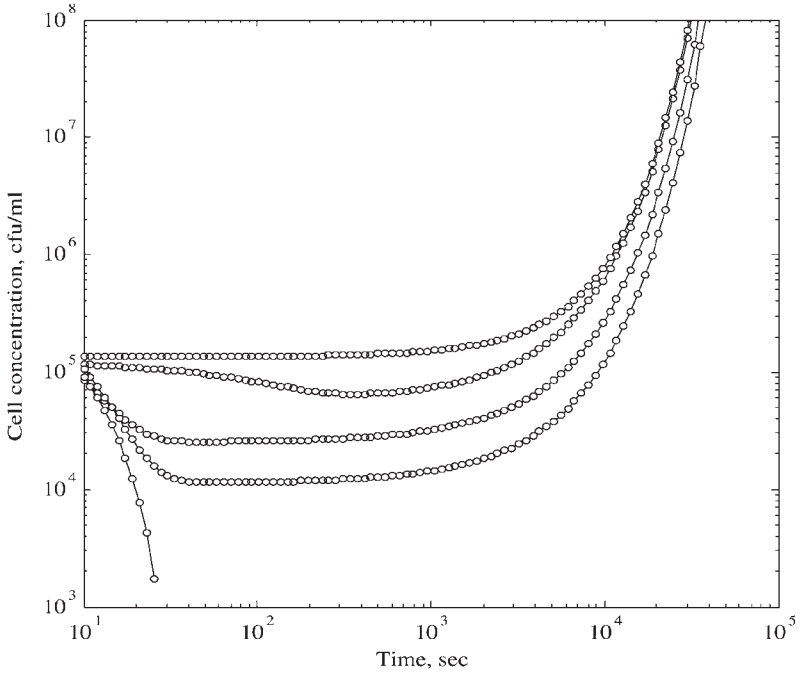

Figure 6. L. monocytogenes *population dynamics as a result of non-steady state nisin release.*

The numerical modeling results are qualitatively in good agreement with the data in reference [6], where the release of nisin from cellulose-based films has been measured and the initial inhibition of *L. monocytogenes* followed by bacteria growth was observed.

DISCUSSION

The optimal antimicrobial packaging system would have a broad antimicrobial spectrum, exert strong antimicrobial activity at low concentrations, have no adverse effects on the food product and packaging material, be cost effective, and satisfy FDA requirements [1]. The type of food, target microorganism, and desired shelf life determine the appropriate AMA and the method of delivery. The present model not only describes the inactivation kinetics of the microbial population under different scenarios, but also allows one to choose the best AMA and the most effective pathogen treatment.

Let us introduce a dimensionless process variable:

$$\alpha = \frac{K_n \gamma}{\mu} \tag{26}$$

The ratio between kinetic constants of bacterial growth and inactivation determines the overall efficacy of the treatment process. Substituting (26) into expressions (13), (17), (21), (25) and rearranging them, one obtained the new set of conditions for effective control of the bacterial population:

$$\left.\begin{array}{c} \dfrac{\alpha}{1+\alpha}\dfrac{1}{\gamma}C_{n0} \\ \dfrac{\alpha}{1+\alpha}\dfrac{1}{\gamma}\dfrac{Q}{\mu} \\ \dfrac{\alpha}{1+\alpha}\dfrac{1}{\gamma}\left(C_{n0}+\dfrac{Q}{u}\right) \\ \dfrac{\alpha}{1+\alpha}\dfrac{1}{\gamma}\left[C_{n0}+\dfrac{Q}{(\mu+\lambda)}\right] \end{array}\right\} \geq C_{c0} \tag{27}$$

Based on this system, it is possible to specify requirements for transport properties and storage capacity of active packaging material for var-

ious regimes of antimicrobial delivery. Obviously, all inequalities in (27) can be rewritten in (27) the generalized form:

$$\frac{\alpha}{\alpha+1}\frac{1}{\gamma} f(C_{n0},\ Q,\ \mu,\ \lambda) \geq C_{c0} \tag{28}$$

where $1/\gamma$ is the AMA "economy" factor specific to the bacteria/AMA pair, i.e. the amount of AMA needed to inactivate one bacterial CFU; $f(C_{n0}, Q, \mu, \lambda) \geq C_{c0}$—the function determined by specific design of the package, packaging material, and food product formulation; $\alpha/(\alpha + 1)$—the coefficient determined by the kinetics of bacteria reproduction and inactivation.

$$\frac{\alpha}{\alpha+1} \rightarrow \begin{cases} 1 \ \text{ for } \ K_n > \mu \\ \dfrac{1}{2} \ \text{ for } \ K_n \sim \mu \\ 0 \ \text{ for } \ K_n < \mu \end{cases} \tag{29}$$

Hence, it is possible to choose an AMA candidate for the food product, which makes the product development and package design processes cost-effective and less time consuming.

The presented model can also be used to predict product shelf life, which can be defined as the time required for bacterial population to grow from its initial level to an unacceptable concentration. Substituting $C_c \rightarrow C_{c\,\mathrm{lim}}$, where $C_{c\,\mathrm{lim}}$ is an acceptable level of bacterial contamination, in (19) and using a Taylor series expansion, one obtains the estimated value of the product shelf life as a function of bacterial growth kinetics and AMA concentration:

$$t_{cr;}\ \frac{C_{c\,\mathrm{lim}}}{1-\alpha\dfrac{C_{n0}}{C_{c0}}} \tag{30}$$

This model provides a direct connection between microbial inhibition in the food system and the release rate of the AMA, and can be used to design more effective controlled-release packaging materials that will improve microbiological safety and quality of food products.

CONCLUSION

In this work, the author attempts to develop analytical model of bacterial population response to adding of an antimicrobial agent as a function of the agent release mode. Although all calculations were performed using nisin as an AMA and *L. monocytogenes* as a model pathogenic microorganism, the model can be applied to various bacteria/AMA systems and used to predict bacterial population dynamics for active packaging applications.

ACKNOWLEDGMENTS

This is publication No. D 10550-2-04 of the New Jersey Agricultural Experiment Station supported by State Funds and the Center for Advanced Food Technology (CAFT). The author wishes to thank Ms. Bernice George for measuring *Listeria monocytogenes* growth kinetics.

REFERENCES

1. A. Brody, L. Kline, and E. Strupinsky, Active Packaging for Food Applications, ed., Technomic Publishing Company., Lancaster, Pennsylvania 2001.
2. M. Madigan, J. Martinko, and J. Brock, Biology of Microorganisms, ed., Pretince Hall 2002.
3. CDC, CDC Press release, www.cdc.gov/od/oc/media/pressrel/r020918b.htm (2002).
4. Y. Kim, H. Paik, and D. Lee, Shelf-life Characteristics of Fresh Oysters and Ground Beef as Affected by Bacteriocin-coated Plastic Packaging Film, *Journal of the Science of Food and Agriculture* 82 (2002) 998–1002.
5. D. S. Cha, K. Cooksey, M. S. Chinnan, and H. J. Park, Release of nisin from various heat-pressed and cast films, *Lebensmittel-Wissenschaft und-Technologie* 36 (2003) 209–213.
6. J. L. Grower, D. K. Cooksey, and K. K. Getty, in WorldPAK-2002, 2002 pp. 981–988 MSU School of Packaging, Lansing, MI.
7. N. Franklin, D. K. Cooksey, and K. K. Getty, in WorldPAK-2002, 2002 pp. 995–999 MSU School of Packaging, Lansing, MI.
8. G. R. Siragusa, C. N. Cutter, and J. L. Willett, Incorporation of Bacteriocin in Plastic Retains Activity and inhibits Surface Growth of Bacteria on Meat, *Food Microbiology* 16 (1999) 229–235.
9. V. Coma, I. Sebti, P. Pardon, A. Deschamps, and P. F.H., Antimicrobial Edible Packaging Based on Cellulosic Ethers, Fatty Acids, and Nisin Incorporation To Inhibit Listeria innocua and Staphylococcus aureus, *Journal of Food Protection* 64 (2001) 470–475.
10. N. Natrajan, and B. W. Sheldon, Inhibition of Salmonella on Poultry Skin using Protein- and Polysaccharide-based Films Containing a Nisin Formulation, *Journal of Food Protection* 63 (2000) 1268–1272.
11. T. Abee, and J. Wouters, Microbial stress response in minimal processing, International *Journal of Food Microbiology* 50 (1999) 65–91.
12. A. M. Driedger, J. L. Rennecker, and B. J. Marinas, Sequential inactivation of

Cryptosporidium parvum oocysts with ozone and free chlorine, *Water Research* 34 (2000) 3591–3597.

13. E. Chasseignaux, P. Gerault, M.-T. Toquin, G. Salvat, P. Colin, and G. Ermel, Ecology of Listeria monocytogenes in the environment of raw poultry meat and raw pork meat processing plants, *FEMS Microbiology Letters* 210 (2002) 271–275.
14. S. Brul, and P. Coote, Preservative agents in foods: Mode of action and microbial resistance mechanisms, *International Journal of Food Microbiology* 50 (1999) 1–17.
15. Y. Chi-Zhang, K. L. Yam, and M. L. Chikindas, Effective control of Listeria monocytogenes by combination of nisin formulated and slowly released into a broth system, *International Journal of Food Microbiology* 90 (2004) 15–22.
16. G. G. Buonocore, M. A. Del Nobile, A. Panizza, M. R. Corbo, and L. Nicolais, A General Approach to Describe the Antimicrobial Agent Release from Highly Swellable Films Intended for Food Packaging Applications., *Journal of Controlled Release.* 90 (2003) 97–107.
17. J. Choi, J. Park, H. Park, and D. Lee, Migration of Preservative from Antimicrobial Polymer Coating into Water., *Food Science and Biotechnology* 10 (2001) 327–330.
18. Y. Kim, D. An, H. Park, J. Park, and D. Lee, Properties of Nisin-incorporated Polymer Coatings as Antimicrobial Packaging Materials., *Packaging Technology and Science* 15 (2002) 247–254.

Effect of γ-Irradiation on Mechanical Properties and Molecular Weight of Thermoformed Polylactic Acid Cups

L.F. VARGAS[1], B.A. WELT[1,*], J. SELIGA[2], P. PULLAMMANAPPALLIL[1], A.B. BRENNAN[2], A.A. TEIXEIRA[1], M.O. BALABAN[1] and C.L. BEATTY[2]

[1]*Packaging Science Program, Agricultural & Biological Engineering Department, University of Florida, PO BOX 110570, Gainesville FL 32611-0570*

[2]*Materials Science and Engineering Department, University of Florida, PO BOX 116400 Gainesville, FL 32611-6400*

ABSTRACT: Effect of gamma irradiation on mechanical properties and molecular weight of polylactic acid (PLA) cups was studied. Shredded and cut samples from cups were exposed to 0, 72 and 172 kGy γ-irradiation. Stress and strain at break were measured on samples (50 mm × 10 mm × 0.15–0.20 mm) using an Instron 4301 with crosshead speed of 30 mm/min. Viscosity and weight average molecular weights were estimated using intrinsic viscosity at 30°C with chloroform as solvent. Mark-Houwink constants of 0.0153/0.0131 ml/g and 0.759/0.777 for k and a, respectively, were used to estimate weight-average/viscosity-average molecular weight of irradiated samples. Results showed reductions in both mechanical properties and molecular weight over the range of doses studied. Stress at break dropped by a factor of 7 and strain at break fell from 75% to 2%. Molecular weight decreased by a factor of 7, suggesting predominance of chain-scission due to irradiation with a scission yield value, G_s, of 2.18.

INTRODUCTION

SUSTAINABLE packaging materials are receiving a lot of attention, and polylactic acid (PLA) is emerging as a leading material in terms of increasing production volumes [1]. Derived from renewable resources such as corn, wood residues and other biomass, PLA is of current interest not only because of the need to replace fossil fuel derived polymers, but also because of its many useful characteristics [2]. However, PLA still has disadvantages such as low melting point, brittle-

*Author to whom correspondence should be addressed. Email: bwelt@ufl.edu

1557-7244/07/03 181-10

ness, instability to environmental conditions and relatively low biodegradation rate. Since PLA is biodegradable under composting conditions, PLA packaging materials are more sensitive to temperature and relative humidity than traditional petroleum based thermoplastics [3,4].

While proponents tout PLA's ability to degrade under composting conditions, rates of biodegradation are relatively low compared to commonly composted organic feedstock. This disparity has the potential to create significant build-up of PLA in commercial/municipal compost process streams, potentially rendering PLA incompatible with such operations. Therefore, there is justification to study complementary treatments that may enhance biodegradation rates of PLA. Several studies focused on effects of electron beam and gamma irradiation on laboratory prepared L and D poly lactides, lactide copolymers and blends [5,6,7]. The objective of this work was to evaluate the potential of γ-irradiation as a post-consumer, pre-composting process in order to rapidly reduce molecular weight and structural integrity of commercially available PLA products prior to composting.

MATERIALS AND METHODS

Materials

Thermoformed PLA drinking cups (Fabri-Kal, Inc., Kalamazoo, MI) were obtained from TREEO Center at the University of Florida. Cup dimensions are shown in Figure 1. Cup walls were clear except for preprinted artwork.

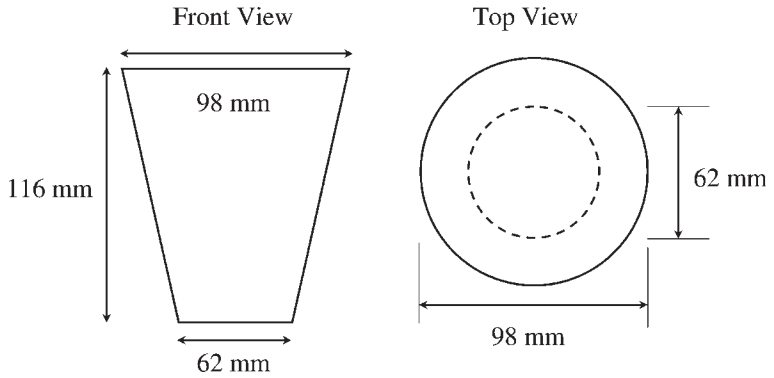

Figure 1. PLA drinking cups drawing.

Irradiation

Shredded and cut PLA samples were irradiated together in a foil lined paperboard canister (73 mm diameter × 180 mm height). The canister was placed inside the irradiation chamber (FL Accelerator Services and Technology, Gainesville, FL) where it was exposed to γ-rays from a Cesium-137 source at a dose rate of 0.78 kGy/h. Samples were irradiated in air in order to promote scission over crosslinking [6,8]. The canister was removed from the irradiation chamber after 92 and 221 hours, and samples achieved absorbed doses of 72 kGy and 172 kGy respectively. Irradiated samples were kept in storage at 25°C for at least 4 days prior to analysis.

Test Samples

For mechanical properties tests, rectangular sheets were prepared in accordance to ASTM D882 [9]. A standard cutter intended for paperboard was used. Specimen dimensions were 10 mm × 50 mm. Sample thickness varied from 150 and 200 μm primarily due to imprecise stretching that is typical of the thermoforming process.

For molecular weight analysis, no specific requirement was needed for dimensions or shape of the PLA samples. PLA cups were shredded into pieces that were about 4mm on edge in order to facilitate uniform irradiation as well as dissolution in chloroform after treatment.

Mechanical Properties

A 4301-Series Instron was used to determine stress and strain at break of treated (72 kGy and 172 kGy) and untreated (0 kGy) PLA rectangular sheets at a temperature of 25°C. The equipment was set at a crosshead speed of 30 mm/min, and the sample set in the machine direction with a gage length of 30 mm. Several repetitions were performed in each tensile test for assure a representative average value of these mechanical properties.

Molecular Weight

The standard method of intrinsic viscosity was used to determine viscosity-average molecular weight and weight-average molecular weight

of PLA samples in accordance to ASTM D2857-95 [10]. Kinematic viscosiy of PLA dilutions (0, 0.1, 0.2, 0.3, 0.4 and 0.5%(v/v)) were determined at 30°C using chloroform as solvent and a calibrated capillary viscosimeter (Cannon-Ubbelodhe Model N°25, Cannon Instrument Company, Inc., State College, PA). These values were used to determine reduced viscosities (μ_{red}) of dilutions and estimate intrinsic viscosities ([μ]) of each treated sample.Viscosity-average molecular weight (M_v) and weight-average molecular weight (M_w) were estimated by the Mark-Houwink (MH) equation (Equation 1).

$$[\mu] = kM^{a} \tag{1}$$

Where constants k and a used for PLA in chloroform at 30°C were 0.0131ml/g and 0.777 for viscosity-average molecular weight (M_v), and 0.0153ml/g and 0.759 for weight-average molecular weight (M_w) [11].

Degree of Chain Scission

The degree of chain scission (G_s) defined as the number of radiolysis events caused by the absorption of 100eV of radiation was calculated by Equation 2 [6].

$$G_s = \frac{N_A\left(\frac{1}{M_n} - \frac{1}{M_{n,0}}\right)}{6.24\times10^{16} D} \tag{2}$$

Where M_n is the number-average molecular weight (g/mol) after irradiation, $M_{n,0}$ is the number-average molecular weight (g/mol) before irradiation, D is the absorbed dose (kGy), and N_A is Avogadro's number (6.023×10^{23}). M_n was assumed to be equal to M_v since doses were below the gel dose [12]. For a constant G_s value, a linearization of $1/M_n - 1/M_{n,0}$ vs. D was done, and the slope of the line used in Equation 2.

RESULTS AND DISCUSSION

Mechanical Properties

PLA made from pure L-Lactide, also called poly(L-lactide), is semi-crystalline. Incorporation or co-polymerization with isomers

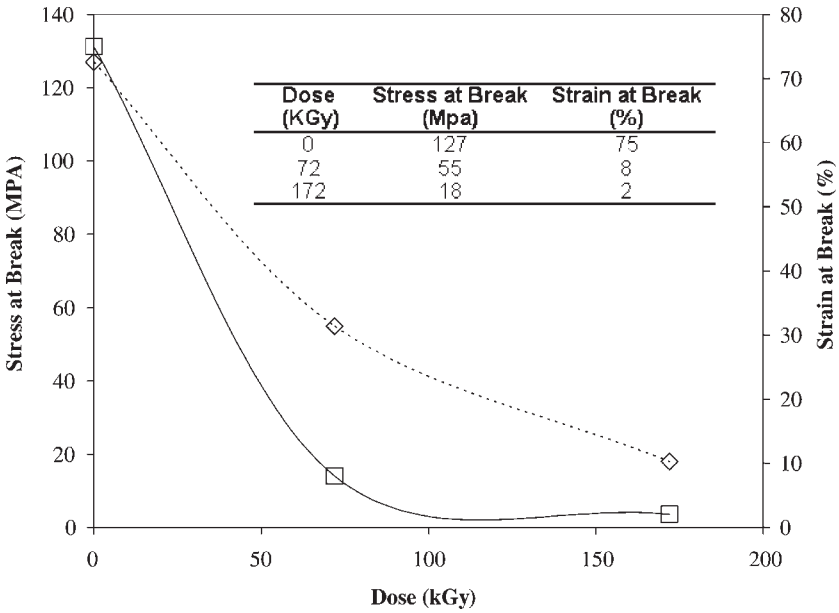

Figure 2. Tensile properties of PLA samples: ◇ stress at break (MPa), □ strain at break (%).

M-lactide or D-lactide decreases degree of crystallinity, causing polymers to become more amorphous [13,14]. PLA resins can be tailor-made for different fabrication processes, including injection molding, sheet extrusion, blow molding, thermoforming, film forming, or fiber spinning. Critical factors include degree of branching, D-isomer content, and molecular weight distribution. For thermoforming, D-isomer content might be in the range of 4–8% [13]. Unirradiated PLA mechanical properties have been studied by other authors and been compared to those of oriented polystyrene (OPS) [15].

Rectangular PLA samples showed increasing brittleness with absorbed dose. At higher doses, samples were sensitive to even careful handling. Results for stress and strain at break using the Instron 4301 are shown in Figure 2.

Higher gamma irradiation doses reduced PLA mechanical properties in a manner that is similar to traditional thermoplastic polymers including polystyrene, polypropylene and polyurethane [16,17,18]. Other authors studied effects of electron beam irradiation on lactides and found similar trends [5,7]. Stress at break of PLA samples irradiated at 172 kGy dropped from 127 MPa to 18 MPa, a factor of about 7. For the same

samples, strain at break dropped from 75% to 2%. These numerical values represent a marked increase in brittleness of the irradiated PLA samples. This behavior suggests crystalline damage due to free radical attack [5]. Poly(lactide)s mainly undergo chain-scissions at doses below 250 kGy. It has been shown, but not confirmed here, that crosslinking reactions increase as a function of the irradiation dose at doses higher than 250 kGy [19].

Molecular Weight

Viscosities of PLA dilutions in chloroform at 30°C increased with polymer concentration (Figure 3) [20]. Higher irradiation doses reduced sample dilution viscosity, confirming chain scission by irradiation exposure.

Results for intrinsic viscosity, [μ], based on reduced viscosities are shown in Figure 4. Intrinsic viscosity is defined as the reduced viscosity projected to zero dilution. Linearity of plots of reduced viscosity throughout the dilution range suggests that concentrations were adequately higher than the dynamic contact concentration, and that solu-

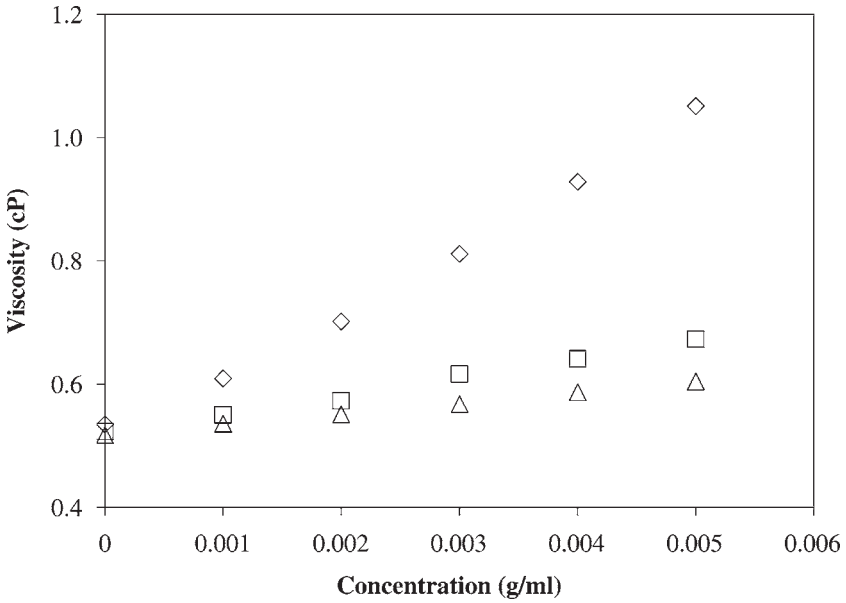

Figure 3. *PLA dilution viscosities: ◇ 0 kGy, □ 72 kGy, △ 172 kGy.*

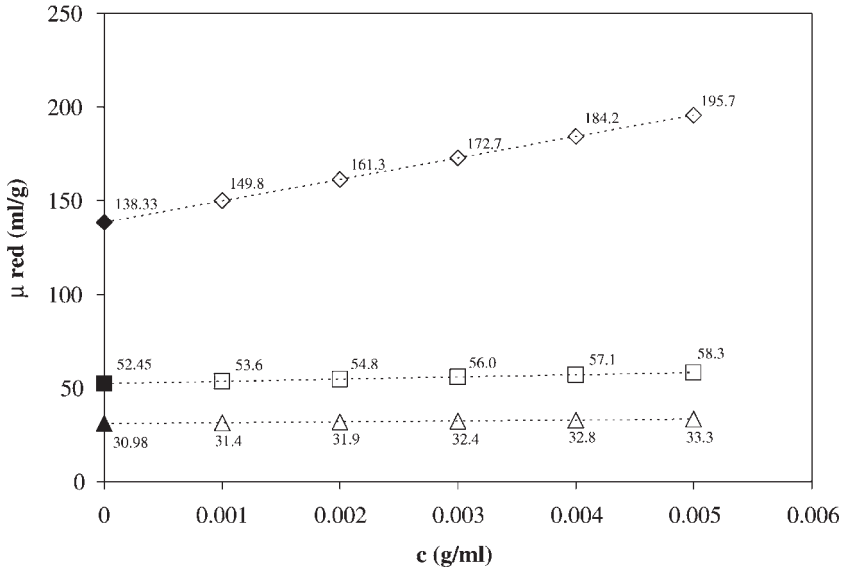

Figure 4. Reduced and intrinsic viscosities for irradiated PLA samples diluted in chloroform at 30°C. ◇ 0 kGy, □ 72 kGy, △ 172 kGy.

tions obeyed the Huggins equation [21]. Hence, our dilutions were above the extremely dilute regime, which satisfies the requirement of the approach used to determine intrinsic viscosity.

Figure 5 shows weight-average (M_w) and viscosity-average (M_v) molecular weights for unirradiated and irradiated PLA samples. Since intrinsic viscosities are lower at higher absorbed doses, molecular weights also conform to the Mark-Houwink equation. This result confirms that chain scission was the predominant effect of tested irradiation treatments. Weight-average molecular weight dropped 86% from 16.3×10^4 to 2.3×10^4. Number-average molecular weight dropped 85% from 15.1×10^4 to 2.2×10^4. These molecular weight reductions were more severe than those found by other authors for poly(L-lactic) acid [6]. This difference may be explained by additional sensitivity of PLA polymer for thermoforming, which also includes D-isomers.

Ratios of weight average to viscosity average molecular weight, M_w/M_v, were 1.08, 1.05 and 1.03 for absorbed doses of 0, 72 and 172 kGy, respectively. These values suggest narrow molecular weight distributions, which would tend to confirm that the origin of our PLA samples was from a ring-opening polymerization process, which is claimed by the PLA manufacturer [13].

Degree of Chain-Scission

The plot of $1/M_n - 1/M_{n,0}$ vs. D is shown in Figure 6. The straight line suggests that chain scission was random [22]. Chain scission yield, G_s, was found to be 2.18, which is greater than values found by other researchers for gamma irradiated poly (L-lactic) acid [6], poly (lactide-co-glycolide) e-beam irradiated and poly (l-lactide) e-beam irradiated [5,6].

CONCLUSION

Irradiation doses up to 172 kGy using Cesium 137 γ-rays affect mechanical properties and molecular weight of commercial polylactic acid. Stress at break and strain at break dropped by factors of 7 and 37, respectively, reflecting the clearly observable increase in brittleness. Molecular weight of polymer irradiated up to 172 kGy dropped in 86%. It was demonstrated that chain scission is the predominant effect of the irradiation process under the evaluated doses, achieving a chain scission yield (G_s) of 2.18. Hence, irradiation process may prove to be an effective pre-composting step to accelerate composting rates of PLA.

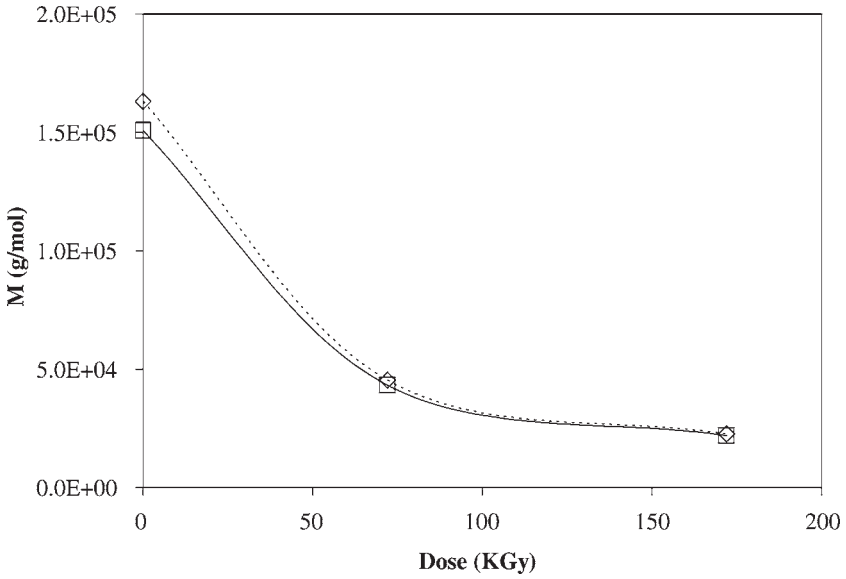

Figure 5. *Molecular weight of PLA samples:* ◇ M_w, □ M_v.

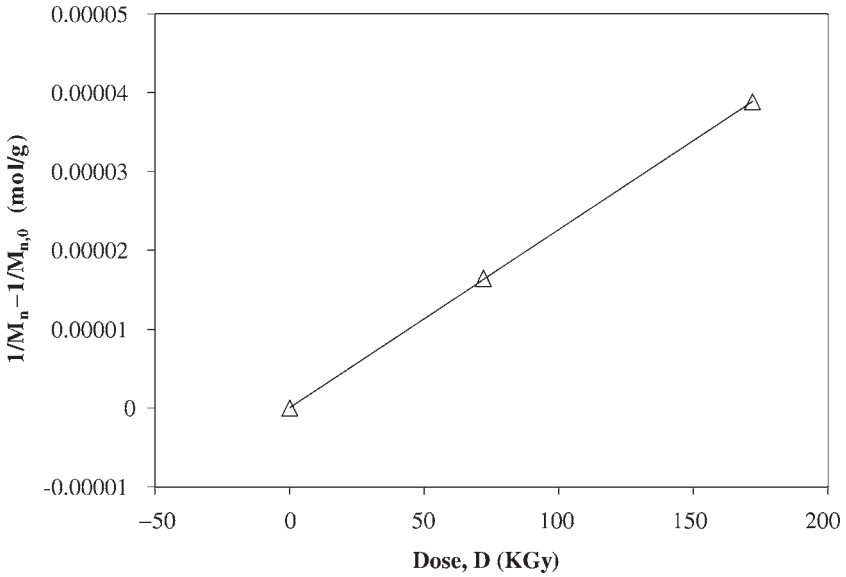

Figure 6. *Plot of* $1/M_n - 1/M_{n,0}$ *against irradiation dose.*

ACKNOWLEDGMENTS

This research was supported by the Institute for Food and Agricultural Sciences (IFAS) at the University of Florida, Gainesville, FL.

REFERENCES

1. Kunioka M., Ninomiya F. and Funabashi M. "Biodegradation of Poly(Lactic Acid) Powders Proposed as the Reference Test Materials for the International Standard of Biodegradation Evaluation Methods". *Polymer Degradation and Stability,* Vol.91, 2006, pp. 1919–1928.
2. Plackett D.V., Holm V.K., Johansen P., Ndoni S., Nielsen P.V., Sipilainen-Malm T., Södergård A. and Verstichel S. "Characterization of L-Polylactide and L-Polylactide–Polycaprolactone Co-Polymer Films for Use in Cheese-Packaging Applications". *Packaging Technology and Science,* Vol.19, 2006, pp. 1–24.
3. Holm V.K., Ndoni S. and Risbo J. "The Stability of Poly(lactic acid) Packaging Films as Influenced by Humidity and Temperature". *Journal of Food Science,* Vol.71, No.2, 2006, pp. 40–44.
4. Ohkita T. and Lee S. "Thermal Degradation and Biodegradability of Poly (lactic acid)/Corn Starch Biocomposites". *Journal of Applied Polymer Science,* Vol.100, 2006, pp. 3009–3017.
5. Loo J.S.C., Ooi C.P., Boey F.Y.C. "Degradation of Poly(Lactide-co-Glycolide) (PLGA) and Poly(L-Lactide) (PLLA) by Electron Beam Radiation". *Biomaterials,* Vol.26, 2005, pp. 1359–1367.
6. Nugroho P., Mitomo H., Yoshii F. and Kume T. "Degradation of Poly(L-Lactic Acid) by γ-Irradiation". *Polymer Degradation Stability,* Vol.72, 2001, pp. 337–343.

7. Ho K. and Pometto A. “Effects on Electron-Beam Irradiation and Ultraviolet Light (365nm) on Polylactic Acid Plastic Films”. *Journal of Environmental Polymer Degradation,* Vol.7, No.2, 1999, pp. 93–100.
8. Hill D.J.T., Milne K.A., O’Donnell J.H. and Pomery P.J. “A Recent Advance in the Determination of Scission and Cross-Linking Yields of Gamma-Ray Irradiated Polymers”. In: *Irradiation of Polymers, Fundamental and Technological Applications.* 1996.
9. ASTM, American Society for Testing and Materials: Standard Test Methods for Tensile Properties of Thin Plastic Sheeting, D882. Annual Book of ASTM. Philadelphia, PA, 1996.
10. ASTM, American Society for Testing and Materials: Standard Practice for Dilute Solution Viscosity of Polymers, D2857-95. Annual Book of ASTM. Philadelphia, PA, 1996.
11. Dorgan J.R., Janzen J., Knauss D.M., Hait S.B., Limoges B., Hutchinson M.H. “Fundamental Solution and Single-Chain Properties of Polylactides”. *Journal of Polymer Science: Part B: Polymer Physics,* Vol.43, 2005, pp. 3100–3111.
12. Busfield W.K. and Watson G.S. “Radiation Chemistry of Polybutene-1”. In: Irradiation of Polymers, *Fundamentals and Technological Applications.* 1996.
13. Drumright R.E., Gruber P.R. and Henton D.E. “Polylactic Acid Technology”. *Advanced Materials,* Vol.23, No.12, 2000, pp. 1841–1846.
14. Karst D. and Yang Y. “Molecular Modeling Study of the Resistance of PLA to Hydrolysis Based on the Blending of PLLA and PDLA”. *Polymer,* Vol.47, 2006, pp. 4845–4850.
15. Auras R.A., Singh S.P. and Singh J.J. “Evaluation of Oriented Poly(Lactide) Polymers vs. Existing PET and Oriented PS for Fresh Food Service Containers”. *Packaging Technology and Science,* Vol.18, 2005, pp.207–216.
16. Bowmer T.N., Cowen L.K., O’Donnell J.H. and Winzor D.J. “Degradation of Polystyrene by Gamma Irradiation: Effect of Air on the Radiation-Induced Changes in Mechanical and Molecular Properties”. *Journal of Applied Polymer Science,* Vol.24, 1979, pp. 425–439.
17. Akin-Oktem G., Tanrisinbilir S. and Tincer T. “Study on Mechanical Properties of Perlite-Filled Gamma-Irradiated Polypropylene”. *Journal of Applied Polymer Science,* Vol.81, 2001, pp. 2670–2678.
18. Shintani H., Kikuchi H. and Nakamura A. “Effects of Gamma-Ray Irradiation on the Change of Characteristics of Polyurethane”. *Journal of Applied Polymer Science,* Vol.41, 1990, pp. 661–675.
19. Södergård A., Stolt M. “Properties of Lactic Acid polymers and their Correlation with Composition”. *Progress in Polymer Science,* Vol.27, 2002, pp. 1123-1163.
20. Schneider M., Claverie J., Graillat C., Mckenna T.F. “High Solids Content Emulsions. I. A Study of the Influence of the Particle Size Distribution and Polymer Concentration on Viscosity”. *Journal of Applied Polymer Science,* Vol.84, 2002, pp. 1878–1896.
21. Du D., Zuo J., An Y., Zhou L. and Liu Y. “Study of Viscosity Abnormality of PS/Toluene Solution in Extremely Dilute Concentration Regime”. *Journal of Applied Polymer Science,* Vol.102, 2006, pp. 4440–4446.
22. Carswell-Pomerantz T., Dong L., Hill D.J.T., O’Donell J.H., Pomery P. “Mechanistic Studies on the Radiation Chemistry of Poly(hydroxybutyrate)”. In: *Irradiation of Polymers, Fundamentals and Technological Aplications.* 1996.

GUIDE TO AUTHORS

1. Manuscripts shall be sent electronically to the editor, Prof. Stanley Dunn at smd@occlusal.rutgers.edu using Microsoft Word in an IBM/PC format. If electronic submission is not possible, three paper copies of double-spaced manuscripts may be sent to Stan Dunn, Editor of the *Journal of Applied Packaging Research*, 98 Brett Road, Piscateway, NJ 08854, USA (Telephone 732-445-4462). Manuscripts should normally be limited to the space equivalent of 6,000 words. The editor may waive this requirement in special occasions. As a guideline, each page of a double-spaced manuscript contains about 300 words. Include on the title page the names, affiliations, and addresses of all the authors, and identify one author as the corresponding author. Because communication between the editor and the authors will be electronic, the email address of the corresponding author is required. Papers under review, accepted for publication, or published elsewhere in journals are normally not accepted for publication in the *Journal of Applied Packaging Research.* Papers published as proceedings of conferences are welcomed.
2. Article titles should be brief, followed by the author's name(s), affiliation, address, country, and postal code (zip) of author(s). Indicate to whom correspondence and proofs should be sent, including telephone and fax numbers and e-mail address.
3. Include a 100-word abstract and keywords.
4. If electronic art files are not supplied, submit three copies of camera-ready drawings and glossy photographs. Drawings should be uniformly sized, if possible, planned for 50% reduction. Art that is sent electronically should be saved in either a .tif or .JPEG files for superior reproduction. All illustrations of any kind must be numbered and mentioned in the text. Captions for illustrations should all be typed on a separate sheet(s) and should be understandable without reference to the text.
5. DEStech uses a numbered reference system consisting of two elements: a numbered list of all references and (in the text itself) numbers in brackets that correspond to the list. At the end of your article, please supply a numbered list of all references (books, journals, web sites etc.). References on the list should be in the form given below. In the text write the number in brackets corresponding to the reference on the list. Place the number in brackets inside the final period of the sentence cited by the reference. Here is an example [2].

   Journal: 1. Halpin, J. C., "article title", *J. Cellular Plastics*, Vol. 3, No. 2, 1997, pp. 432–435.
   Book: 2. Kececioglu, D. B. and F.-B. Sun. 2002. *Burn-In Testing: Its Quantification and Optimization*, Lancaster, PA: DEStech Publications, Inc.

6. Tables. Number consecutively and insert closest to where first mentioned in text or type on a numbered, separate page. Please use Arabic numerals and supply a heading. Column headings should be explanatory and carry units. (See example at right.)

Table 5. Comparison of state-of-the-art matrix resins with VPSP/BMI copolymers.

Resin System	Core Temp. (DSC peak)	Char Yield, %
Epoxy (MY720)	235	30
C379: H795 = 1.4	285	53

7. Units & Abbreviations. SI units should be used. English units or other equivalents should appear in parentheses if necessary.
8. Symbols. A list of symbols used and their meanings should be included.
9. Page proofs. Authors will receive page proofs by E-mail. Proof pages will be in a .PDF file, which can be read by Acrobat Reader. Corrections on proof pages should be limited to the correction of errors. Authors should print out pages that require corrections and mark the corrections on the printed pages. Pages with corrections should be returned by FAX (717-509-6100) or mail to the publisher (DEStech Publications, Inc., 1148 Elizabeth Ave., #2, Lancaster, PA 17601, USA). If authors cannot handle proofs in a .PDF file format, please notify the editor, Stan Dunn at smd@occlusal.rutgers.edu.
10. Index terms.With proof pages authors will receive a form for listing key words that will appear in the index. Please fill out this form with index terms and return it.
11. Copyright Information. All original journal articles are copyrighted in the name of DEStech Publications, Inc. All original articles accepted for publication must be accompanied by a signed copyright transfer agreement available from the journal editor. Previously copyrighted material used in an article can be published with the *written* permission of the copyright holder (see #14 below).
12. Headings. Your article should be structured with unnumbered headings. Normally two headings are used as follows:

    Main Subhead: DESIGN OF A MICROWAVE INSTALLATION
    Secondary Subhead: Principle of the Design Method

    If further subordination is required, please limit to no more than one (*Third Subhead*).

13. Equations. Number equations with Arabic numbers enclosed in parentheses at the right-hand margin. Type superscripts and subscripts clearly above or below the baseline, or mark them with a caret. Be sure that all symbols, letters, and numbers are distinguishable (e.g., "oh" or zero, one or lowercase "el," "vee" or Greek nu).
14. Permissions. The author of a paper is responsible for obtaining releases for the use of copyrighted figures, tables, or excerpts longer than 200 words used in his/her paper. Copyright releases are permissions to reprint previously copyrighted material. Releases must be obtained from the copyright holder, which is usually a publisher. Forms for copyright release will be sent by the editor to authors on request.

General: The *Journal of Applied Packaging Research* and DEStech Publications, Inc. are not responsible for the views expressed by individual contributors in articles published in the journal.